International Journal of Computational Methods and Experimental Measurements
https://www.acadlore.com/journals/IJCMEM

# Design and Performance Analysis of a Conical Fluidized Bed Dryer for Small-Scale Coffee Drying

Elder Mendoza Orbegoso[1], Raul La Madrid Olivares[2], Daniel Marcelo-Aldana[2], Andy S. Mendoza[3], Nattan Roberto Caetano[4], Giulio Lorenzini[5*]

[1] Departamento de Ingeniería Mecatrónica, Facultad de Ingeniería, Universidad Nacional de Trujillo, 13001 Trujillo, Peru
[2] Laboratorio de Energía, Universidad de Piura, 20009 Piura, Peru
[3] Programa de Ingeniería Mecatrónica, Facultad de Ingeniería, Universidad Privada del Norte, 13001 Trujillo, Peru
[4] Departamento de Engenharia Mecânica, Universidade Federal de Santa Maria, 97105-900 Santa Maria, Brazil
[5] Dipartimento di Ingegneria dei Sistemi e delle Tecnologie Industriali, Università di Parma, 43124 Parma, Italy

* Correspondence: Giulio Lorenzini (giulio.lorenzini@unipr.it)

**Received:** 03-18-2026 **Revised:** 04-22-2026 **Accepted:** 06-03-2026

**Citation:** E. M. Orbegoso, R. La Madrid Olivares, D. Marcelo-Aldana, A. S. Mendoza, N. R. Caetano, and G. Lorenzini, "Design and performance analysis of a conical fluidized bed dryer for small-scale coffee drying," *Int. J. Comput. Methods Exp. Meas.*, vol. 14, no. 2, pp. 314–342, 2026. https://doi.org/10.56578/ijcmem140210.



**Abstract:** Small-scale coffee producers require drying systems that reduce dependence on weather, improve moisture uniformity and remain technically feasible at laboratory or farm scale. This work presents the design and performance analysis of a conical fluidized-bed dryer (FBD) for parchment coffee, focusing on the reactor geometry, air-distribution strategy, heating-chamber configuration and electric-resistance arrangement. The experimental stage included blower characterization from 10 to 60 Hz, with measured outlet air velocities from 4.8 to 35.5 m/s and volumetric flow rates from 0.0098 to 0.0725 $m^3/s$. Fluidization observations were performed with parchment-coffee masses of 0.5, 3.0, 4.0 and 5.0 kg. The numerical stage, developed in SolidWorks Flow Simulation, compared cylindrical and conical reactor configurations, distributor alternatives, conical opening angles of 20°, 25° and 30°, heating-chamber geometries, baffle arrangements and electrical-resistance layouts. The cylindrical prototype showed non-uniform fluidization because the incoming jet expanded poorly and remained attached to one side of the reactor, producing localized high-velocity regions and stagnant zones. In contrast, the conical reactor promoted grain recirculation toward the lower high-velocity region and was therefore selected for the final design. The proposed dryer uses a 25° conical reactor, a 50.8 mm inlet section, a 152.4 mm heating chamber with conical inlet and outlet sections, a flat baffle and four 900 W spiral electrical resistors. The ideal heating demand was estimated as 3.40 kW for increasing the air temperature from approximately 30 °C to 70 °C, while the installed 3.60 kW heater capacity provides a 5.9% margin relative to the ideal requirement. The results demonstrate the design feasibility of a 5 kg parchment-coffee fluidization capacity. However, drying kinetics, pressure drop, energy consumption, final moisture uniformity and calibrated uncertainty must still be validated experimentally in the constructed prototype.

**Keywords:** Fluidized bed dryer; Parchment coffee; Small-scale drying; Electric heating; Air distribution

## 1 Introduction

Drying is one of the most critical post-harvest operations in coffee processing because the final moisture content determines storage stability, microbial safety, transportation suitability and commercial quality. In parchment coffee, insufficient or non-uniform drying favours microbial growth, quality deterioration and moisture reabsorption during storage, whereas excessive drying may reduce product mass and affect the economic return to the grower. In many coffee-producing regions, including Peru, traditional sun drying remains widely used because it is inexpensive and simple to implement; however, it is highly dependent on weather, requires frequent manual handling, exposes the product to environmental contamination, and may take approximately 12 to 15 days under local conditions [1]. From an engineering perspective, coffee drying is a simultaneous heat and mass transfer process in which the drying rate depends on the interaction among air temperature, relative humidity, airflow distribution, bed depth, particle properties and residence time [2, 3]. Therefore, the development of compact dryers with controlled airflow and temperature is especially relevant for small-scale producers who require faster, more uniform and more reproducible drying processes.

Several artificial drying technologies have been proposed to reduce the limitations of open sun drying. Tray dryers, rotary dryers, tunnel dryers, fixed-bed dryers, solar or hybrid solar dryers, microwave-assisted dryers and fluidized-bed dryers (FBDs) have all been considered for agricultural products and coffee beans. Soeswanto et al. [4] reviewed coffee drying technologies and concluded that the selection of drying air temperature and relative humidity is decisive for microbiological safety, beverage quality and energy consumption. Their review also showed that drying at approximately 50 °C may provide a better compromise between drying time and coffee quality than lower-temperature drying, while microwave-based techniques can shorten the process but may introduce temperature non-uniformity. Similarly, Asrate and Ali [5] emphasized that food-drying performance is strongly affected by dryer type, airflow distribution and operating parameters, and that computational fluid dynamics (CFD), response surface methodology, artificial neural networks and other optimization tools are increasingly used to improve equipment design and process control.

Among the available artificial drying technologies, FBDs have attracted particular interest for granular agricultural products because they promote direct contact between the hot air and the solid particles. In a fluidized bed, the upward air stream suspends the material and causes the particle bed to behave similarly to a fluid [6]. This condition increases the exposed surface area of the product, improves heat and mass transfer, reduces temperature gradients inside the bed and can lead to faster and more uniform moisture removal than static-bed systems [7, 8]. Nevertheless, the advantages of fluidized-bed drying are strongly dependent on the hydrodynamic behavior of the bed. Poor distributor design, inappropriate reactor geometry or excessive bed cross-sectional area may produce air channeling, particle segregation, dead zones, local hot spots and non-uniform drying [7]. For this reason, the geometric design of the reactor and the airflow path is not a secondary aspect of the dryer but a central design variable.

Previous studies on fluidized-bed drying of agricultural products have demonstrated that operating variables and geometry substantially affect both performance and product quality. Nazghelichi et al. [9] investigated carrot-cube drying and showed that inlet air temperature, bed depth and particle size influence energy and exergy efficiency. Reyes et al. [10] analyzed pulsed fluidized-bed drying of broccoli and found that air temperature, airflow rate, plate rotation speed and particle size modify drying kinetics and quality-related attributes, including antioxidant capacity and polyphenol retention. Soponronnarit et al. [11] optimized soybean drying by combining drying-rate equations and quality models, concluding that drying temperature, bed depth, air velocity and air recirculation must be jointly adjusted to balance capacity, energy consumption and product quality. In the case of paddy drying, Das et al. [12] compared cylindrical and conical fluidized-bed configurations and reported that conical geometries and spiral flow-promoting devices can improve drying characteristics and energy behavior. These studies support the idea that fluidized-bed drying should be designed by integrating product properties, airflow distribution and reactor geometry rather than by merely scaling a cylindrical column.

Coffee-specific studies further confirm the relevance of controlled drying and fluidization. López Fontal [13] designed and constructed a 5 kg coffee fluidized-bed prototype and reported homogeneous final moisture distribution, with differences below 0.86%, showing that fluidized-bed drying can be a feasible alternative to static mechanical drying for coffee. Unigarro Bolaños [14] experimentally evaluated the effect of temperature and air velocity on coffee drying time and reported shorter drying periods than traditional methods, while maintaining final moisture differences below 1%. More recently, Konsil et al. [15] analyzed the performance of a designed FBD for coffee beans and confirmed the applicability of this technology for coffee drying. Wahyuni et al. [16] studied a pilot-scale FBD assisted with zeolite adsorbent using 500 g of Arabica coffee, air temperatures of 40, 50, and 60 °C, and an average air velocity of 4.91 m/s; they reported that 50 °C reduced the moisture content from 28% to 12.45% in 3 h, while the use of zeolite reduced drying time by 11%. This result is particularly relevant because it demonstrates that moisture removal can be enhanced not only by increasing temperature but also by improving the moisture-absorbing capacity of the air stream.

Other recent coffee-drying studies show alternative routes for process intensification and energy improvement. Reyes-Chaparro et al. [17] studied parchment coffee drying using combined fluidization and microwave heating, showing that microwave assistance can accelerate drying, whereas fluidization helps control sample temperature and reduce thermal heterogeneity. However, this approach is technologically more complex than conventional hot-air systems and may require more sophisticated control to avoid uneven heating. Suherman et al. [18] evaluated a photovoltaic-direct solar dryer for coffee beans at drying temperatures of 40, 45 and 50 °C, reporting that 50 °C was the optimum condition and that the system could reduce coffee moisture to below 12.5% within 12 to 16 h from an initial moisture content of 45%. Their energy and exergy results highlight the potential of renewable-energy dryers, but the system principle differs from electrically heated fluidized-bed drying and depends strongly on solar resource availability.

In addition to experimental studies, numerical modeling has become an important tool for analyzing and improving dryer design. Baidhe and Clementson [19] reviewed modeling and simulation in grain and seed drying systems and concluded that such approaches are useful for optimizing drying procedures, simulating air and particle flow, implementing process controls and assessing quality-related changes. However, they also noted that the range of grains and dryer configurations evaluated in the literature remains limited. This observation is relevant for coffee drying because parchment coffee has specific geometric, density and porosity characteristics that affect the onset of fluidization and the risk of air channeling. Accordingly, numerical simulation should be combined with experimental observation to evaluate whether a proposed reactor geometry can provide adequate airflow distribution for the target coffee mass.

Recent modeling and control-oriented studies further support the need to combine experimental observation with numerical design tools in drying equipment. Tu et al. [20] coupled CFD simulation with experimental measurement in FBD and showed that wet-particle drying is strongly affected by the evolution of particle moisture, internal circulation and gas-solid heat and mass transfer. De Munck et al. [21] demonstrated that computational fluid dynamics-discrete element method (CFD-DEM) coarse-graining can reduce the computational cost of fluidized-bed drying simulations while preserving key quantities such as particle temperature, density and Sherwood-number trends. For packed-bed drying, Tran and Le [22] reported that CFD can reveal strong maldistribution of temperature and moisture content, reinforcing the importance of airflow uniformity in granular beds. Arsenoaia et al. [23] designed and assessed an innovative seed dryer using CFD and SolidWorks, showing that internal deflectors can improve drying-agent distribution and reduce heat release and energy consumption. Coffee-specific studies also confirm the relevance of controlled airflow and temperature: Yuwana and Syafnil [24] evaluated a tandem hybrid solar-biomass dryer for coffee cherry drying, while Nafisah et al. [25] showed that fuzzy temperature control in a Robusta coffee-bean dryer can stabilize drying at 50 °C and reach 12% moisture content. These works reinforce the relevance of the present design approach, in which reactor geometry, flow distribution and heating configuration are treated as coupled design variables.

Table 1 summarizes representative previous works and identifies the limitations that motivate the present study. Overall, the literature indicates that fluidized-bed drying can improve heat and mass transfer, reduce drying time and improve moisture uniformity. However, many studies focus on drying kinetics after the dryer geometry has already been selected, use lower batch masses than those required for small-scale coffee processing, or employ more complex hybrid systems such as microwave or solar-assisted dryers. In addition, previous works often provide limited discussion of the design process used to select the reactor geometry, air distributor, heating chamber and heater arrangement.

**Table 1.** Summary of previous drying studies, main findings and remaining gaps relevant to the proposed coffee fluidized-bed dryer (FBD)

| Reference | System/Product | Relevant Variables or Scope | Main Finding | Limitation or Gap for the Present Work |
|---|---|---|---|---|
| [7] | Fluidised-bed drying of agro-products | Review of process advantages and drawbacks | FBDs provide high heat and mass transfer, rapid drying and improved moisture uniformity | General review; not focused on a specific 5 kg coffee prototype |
| [6] | Hot-air fluidized-bed drying design | Design fundamentals for fluidization and airflow calculations | Provides a theoretical basis for estimating air velocity and dryer dimensions | Requires adaptation to parchment-coffee properties and local prototype constraints |
| [12] | Paddy drying in cylindrical and conical FBDs | 1–3 kg batches; cone angle and spiral device | Conical configurations improved drying characteristics and energy behavior | Rice/paddy application; smaller mass than the 5 kg coffee target |
| [13] | Coffee FBD prototype | 5 kg coffee capacity | Reported homogeneous final moisture, with differences below 0.86% | Limited detail on heating-chamber optimization and airflow-geometry selection |
| [15] | Designed FBD for coffee beans | Performance analysis of coffee-bean drying | Confirms the relevance of FBD technology for coffee drying | Different prototype scale and configuration |

| | | | | |
|---|---|---|---|---|
| [4] | Review of coffee-drying technologies | Tray, rotary, fluidized-bed, microwave and hybrid options | Emphasized proper selection of temperature and relative humidity; 50 °C was identified as an efficient condition in reviewed studies | Review article; does not develop a new 5 kg conical prototype |
| [16] | Pilot-scale FBD assisted with zeolite | 500 g Arabica coffee; 40, 50, and 60 °C; 4.91 m/s | At 50 °C, moisture decreased from 28% to 12.45% in 3 h; zeolite reduced drying time by 11% | Focused on process performance and air dehumidification, not conical reactor geometry |
| [17] | Parchment coffee with combined fluidization and microwave heating | Drying curves and thermal imaging | Microwave assistance intensified drying, while fluidization helped control temperature distribution | More complex technology than a low-complexity electrically heated hot-air prototype |
| [18] | Photovoltaic-direct solar coffee dryer | 40, 45, and 50 °C; energy and exergy analysis | 50 °C was the optimum condition; moisture below 12.5% was achieved in 12–16 h | Different energy source and dryer principle; performance depends on solar availability |
| [5] | Food-dryer technologies and optimization methods | Review of dryer types, CFD, artificial neural networks, ANOVA, RSM and optimization tools | Highlighted the need to optimize dryer type, airflow distribution and operating parameters | Broad review; system-specific experimental validation remains necessary |
| [19] | Modeling and simulation of grain/seed drying | Air/particle flow, quality modeling and process control | Demonstrated the usefulness of modeling and simulation for dryer design and quality assessment | General grain/seed review; not specific to parchment coffee or conical FBDs |
| [20] | Wet-particle drying in FBD | CFD simulation coupled with experimental measurement; particle moisture evolution, internal circulation and gas-solid heat and mass transfer | Showed that CFD can capture key drying mechanisms in fluidized beds and that wet-particle drying depends strongly on particle circulation and gas-solid transport | Focused on wet particles in a general FBD; not a coffee-specific 5 kg conical prototype |
| [21] | CFD-DEM simulation of fluidized-bed drying | Coarse-graining technique for reducing computational cost while modeling particle-scale drying | Demonstrated that coarse-grained CFD-DEM can preserve relevant trends in particle temperature, particle density and Sherwood number while reducing computational demand | Advanced multiphase modeling approach; not implemented in the present SolidWorks design-stage simulations |
| [22] | Packed-bed drying process | CFD analysis of particle properties, drying conditions and lateral edge heating modes | Reported that CFD can reveal non-uniform temperature and moisture distributions in granular beds, reinforcing the importance of airflow distribution | Packed-bed rather than fluidized-bed system; not specific to coffee or conical fluidization |

| | | | | |
|---|---|---|---|---|
| [23] | Innovative seed dryer | CFD/SolidWorks-based design assessment; internal deflectors and drying-agent distribution | Showed that internal deflectors can improve drying-agent distribution and may reduce heat release and energy consumption | Seed-dryer application; does not evaluate parchment coffee fluidization or the present conical reactor geometry |
| [24] | Tandem hybrid solar-biomass dryer for coffee cherry | Solar-biomass drying of coffee cherries; performance evaluation of a hybrid energy dryer | Demonstrated that hybrid solar-biomass drying can improve coffee-cherry drying performance without relying only on grid electricity | Different drying principle and energy source; focuses on coffee cherry rather than parchment-coffee fluidization |
| [25] | Robusta coffee-bean rotary dryer | Fuzzy logic temperature control; drying stabilisation around 50 °C and final moisture target | Showed that fuzzy temperature control can stabilize coffee drying and help reach approximately 12% moisture content | Rotary dryer and control-system study; not focused on fluidized-bed geometry or airflow distribution in a conical reactor |

Note: FBD = fluidized-bed dryer; CFD = computational fluid dynamics; ANOVA = analysis of variance; RSM = response surface methodology; DEM = discrete element method.

Based on these gaps, the originality of the present work lies in the design and performance analysis of a conical FBD intended to fluidize up to 5 kg of parchment coffee using a blower available in a laboratory prototype and an integrated electrically heated air chamber. Unlike studies that focus mainly on drying kinetics under a fixed geometry, this work treats the geometric configuration as a key design problem. Cylindrical and conical reactor behaviors, distributor alternatives, heating-chamber geometry and heater arrangement are evaluated through experimental observation and SolidWorks Flow Simulation. The practical purpose is to develop a compact, technically feasible prototype for small-scale coffee drying in northern Peru, while providing a design basis that can later be validated through drying curves, moisture uniformity, energy consumption and product-quality measurements.

## 2 Methodology

The methodology was divided into two complementary parts. The experimental methodology was used to identify the limitations of an existing cylindrical fluidized-bed prototype and to define the physical constraints of the new design. The numerical methodology was used as a design-screening tool to compare airflow patterns in different reactor, distributor, heating-chamber and heater configurations.

### 2.1 Experimental Methodology

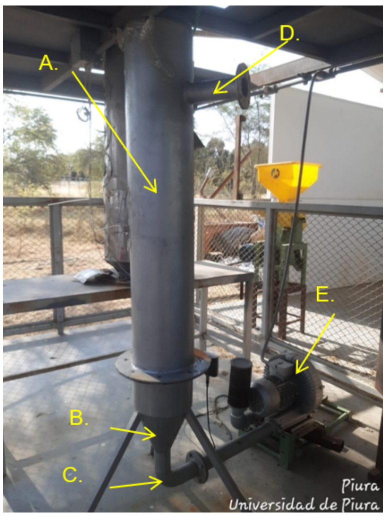


**Figure 1.** Existing cylindrical fluidized-bed dryer (FBD) used as the baseline experimental system: A. cylindrical reactor; B. conical lower transition section; C. vertical inlet/elbow; D. 50.8 mm outlet pipe; F. centrifugal blower

The baseline equipment was the FBD installed at the University of Piura, as ca be seen in Figure 1. This prototype consists of a blower, a horizontal 2 in outlet pipe, an elbow that redirects the air stream vertically, and a cylindrical reactor of approximately 215–220 mm diameter and 1000 mm height. The blower was operated through a frequency-control system available in the previous prototype, which allowed the air supply to be evaluated from 10 to 60 Hz. The outlet pipe diameter was used to calculate the volumetric flow rate from the measured average velocity.

The coffee used in the experimental screening was parchment coffee from Canchaque, Piura, with an initial moisture content of 56% wet basis. The work focused on the fluidization capability of the system rather than on a completed drying run. The tests considered masses of 0.5 kg, 3 kg, 4 kg and 5 kg. A digital anemometer integrated in the prototype was used to record air velocity values, while a balance was used for the sample masses.

#### 2.1.1 Blower frequency control

Table 2 shows the frequency sweep of the blower showed that increasing frequency increased both the pipe velocity and the volumetric flow rate. At 60 Hz, the measured pipe velocity was 35.5 m/s and the corresponding volumetric flow rate was 0.0725 $m^3$/s. At 10 Hz, the velocity and volumetric flow rate were 4.8 m/s and 0.0098 $m^3$/s, respectively. These data were used as inlet conditions for the subsequent numerical studies.

**Table 2.** Blower characterization from 10 to 60 Hz: measured pipe air velocity and calculated volumetric flow rate

| Frequency (Hz) | Air Velocity (m/s) | Volumetric Flow Rate ($m^3$/s) | Volumetric Flow Rate ($m^3$/h) |
|---|---|---|---|
| 10 | 4.8 | 0.0098 | 35.30 |
| 15 | 7.1 | 0.0145 | 52.21 |
| 20 | 9.5 | 0.0194 | 69.86 |
| 25 | 12.5 | 0.0255 | 91.93 |
| 30 | 16.9 | 0.0345 | 124.29 |
| 35 | 20.6 | 0.0421 | 151.50 |
| 40 | 22.3 | 0.0456 | 164.00 |
| 45 | 26.0 | 0.0531 | 191.21 |
| 50 | 29.1 | 0.0594 | 214.01 |
| 55 | 31.9 | 0.0652 | 234.60 |
| 60 | 35.5 | 0.0725 | 261.07 |

#### 2.1.2 Reactor and bed tests

Cylindrical-reactor tests showed that air expansion into the large reactor cross-section did not produce uniform fluidization. As shown in Table 3, the digital anemometer, located in an expanded area of approximately 0.036 $m^2$, indicated about 1.6 m/s at 60 Hz, whereas a simple area-based estimate suggested approximately 2 m/s. This discrepancy was consistent with the flow visualization: air moved preferentially close to the lateral wall instead of expanding uniformly through the bed. With 500 g of coffee, the grains vibrated at low frequencies, began to levitate in a lateral zone near 35 Hz, fluidized in two directions at 50 Hz and remained non-uniform at 60 Hz. With 3 kg, fluidization was more visible but still incomplete. These observations motivated the transition from a cylindrical reactor to a conical reactor.

**Table 3.** Experimental fluidization response of 500 g of parchment coffee in the cylindrical reactor at different blower frequencies

| Frequency (Hz) | Measured Velocity (m/s) | Observed Behavior |
|---|---|---|
| 20 | 0.8 | No fluidization |
| 30 | 1.6 | Slight grain vibration |
| 32 | 2.0 | Slight grain vibration |
| 35 | 2.6 | Air starts to levitate grains in a lateral zone |
| 38 | 3.3 | The pushed air changes zone |
| 40 | 3.5 | Grains float and fall toward the end region |
| 50 | 4.6 | Fluidization in two directions |
| 60 | 5.4 | Fluidization remains non-uniform |

Conical testing was carried out by adapting provisional conical structures to the existing prototype. A conical form with insufficient opening compressed the 5 kg mass and prevented the air from lifting the bed. A larger opening, close to 25°, produced the expected circulation: coffee grains lifted in the high-velocity zone and returned by gravity through lower-velocity zones. This behavior was used to define the conical reactor as the basis of the proposed design.

### 2.1.3 Physical properties and design equations

The theoretical minimum-fluidization estimate used the physical properties reported for parchment coffee and air at the representative average temperature of 50 °C. Parchment coffee was represented by an equivalent diameter of 8.55 mm and an apparent density of 391.44 kg/m$^3$. Air properties at 50 °C were taken as $\rho$ = 1.092 kg/m$^3$ and $\mu$ = 1.963 × 10$^{-5}$ kg/(m·s). Following the fluidized-bed drying design approach described by Patil and Kadam [6], the simplified minimum-fluidization estimate was calculated as:

$$U_{mf} = 0.00137 \frac{(\rho_s - \rho)\, gd^2}{\mu} \tag{1}$$

where, $\rho_s$ and $\rho$ are the density of the coffee beans and the density of the fluid, $g$ is the gravity, $d$ is the equivalent diameter found experimentally and $\mu$ is the dynamic viscosity of the fluid. With the above data, the theoretical value is $U_{mf} = 19.53\ \mathrm{m/s}$. This value was used as a design target for the bed region, recognising that the effective velocity in a real dryer depends on geometry, distributor resistance and local flow paths. The superficial velocity was calculated as:

$$U_0 = Q/A \tag{2}$$

Eq. (2) follows from the definition of superficial gas velocity used in fluidized-bed design [6]. This equation explains why increasing the bed diameter in the cylindrical prototype reduced the average velocity and promoted non-uniform fluidization. The proposed design therefore keeps the lower bed region close to the blower outlet scale, while allowing the conical section to provide the volume required for a 5 kg batch. The 5 kg parchment-coffee mass occupied approximately 0.0072 m$^3$. For a 25° conical reactor and a lower diameter close to the 2 in inlet, the required conical height was estimated to be at least 440 mm. A 300 mm cylindrical upper cover was added to provide freeboard so that moving grains do not hit the top surface.

### 2.1.4 Fluidization tests in conical reactor

As evidenced in the scientific literature, conical reactors exhibit superior thermodynamic performance in comparison to their cylindrical counterparts. Furthermore, the centering of the motive force allows the grains to be levitated from the center, directing them toward the side wall. This, in turn, results in the creation of spaces that are occupied by nearby grains due to the gravitational force. This phenomenon is illustrated in Figure 2. Although the thrust exerted by the air is not centered and is still directed to the side, the suggested conical section will allow the fluidization behavior described above to be obtained. This guarantees that all the grains will receive the hot airflow, ensuring uniformity in the drying process. In order to study the behavior of the airflow in a conical reactor, experimental fluidization tests were carried out on a provisional conical structure.

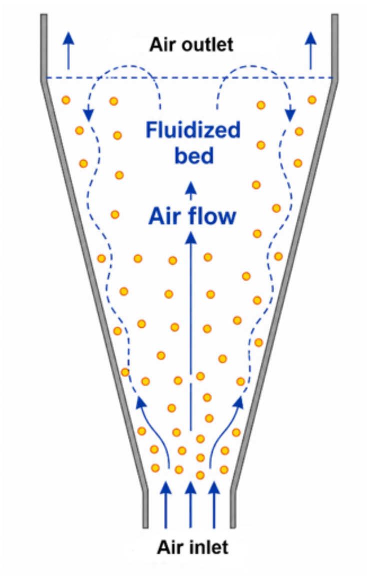


**Figure 2.** Expected grain-circulation mechanism in the conical reactor: upward motion in the high-velocity region and downward return through lower-velocity zones

To evaluate whether a conical reactor could overcome the wall-attached jet observed in the cylindrical prototype, three exploratory fluidization tests were performed using provisional conical structures. First, the original distributor was retained to observe whether the conical wall could redirect grain motion toward the lower high-velocity region. Second, a narrow conical structure was tested to evaluate the effect of bed compression at low opening angle. Third, a wider conical structure, close to a 25° opening angle, was tested with the target 5 kg coffee mass. These tests were used as design-screening experiments rather than complete drying runs, and the observed grain motion was later used to define the numerical design cases.

Figure 3a shows the conical reactor concept; the air distributor of the prototype was initially used. This resulted in a more turbulent motion of the coffee beans, as can be seen in Figure 3b. The airflow still exhibited a tendency to follow the lateral surface; however, the conical geometry allowed beans from regions without significant flow to migrate toward the bottom, where they subsequently became fluidized.


(a)

(b)

**Figure 3.** Preliminary conical-structure test: (a) distributor used in the prototype; (b) top view of the induced grain motion

A small conical reactor was then constructed (see Figure 4). In this design, however, the diameter did not increase appreciably along the reactor length. Consequently, when tested with 5 kg of coffee, the beans became compressed, and the air was unable to fluidize them. In contrast, when a 500 g mass was used, the beans fluidized readily.


**Figure 4.** Fluidization test in a narrow conical structure, showing limitations when the 5 kg coffee mass becomes compressed

Finally, a cone with a larger opening angle was built (see Figure 5), yielding the expected outcome. The minimum fluidization velocity was approximately 19 m/s, which proved sufficient to fluidize the 5 kg mass. After completing the fluidization tests, it was concluded that the optimal reactor geometry is conical, with further refinement possible through the use of simulation software.


**Figure 5.** Fluidization test in a wider conical structure, showing improved grain motion for the 5 kg coffee mass

## 2.2 Numerical Methodology

The numerical methodology was carried out through CFD based simulations in order to support the design of the airflow path, the heating chamber and the conical fluidized-bed reactor before prototype construction. The objective of this subsection was not to predict the complete drying kinetics of parchment coffee, but to compare alternative geometries in terms of airflow distribution, velocity recovery, recirculation tendency, thermal-field uniformity and the ability of the proposed system to deliver hot air to the bed region. Therefore, the simulations were used as a comparative design tool, and the final design decisions were based on the combined interpretation of experimental fluidizations observations and numerical airflow patterns.

The three-dimensional geometries were developed in SolidWorks and analyzed using SolidWorks Flow Simulation. Each dryer configuration was treated as an internal-flow problem. For this purpose, the openings of the computational domain were sealed with lids, allowing the inlet and outlet boundary conditions to be assigned directly to the corresponding faces. The computational domain included the blower outlet pipe, the heating chamber, the internal deflector, the curved elbow, the distributor or mesh-support region, the conical reactor and the upper outlet. The baseline simulation of the previous prototype was performed using an inlet volumetric flow rate of 0.070 $m^3/s$ and an atmospheric-pressure outlet. The parametric simulations considered inlet flow rates of 0.070, 0.065, 0.059, 0.053 and 0.046 $m^3/s$, corresponding to the operating range obtained experimentally from the blower frequency sweep.

### 2.2.1 Governing equations and turbulence modeling

The airflow was modeled as a continuous Newtonian gas phase. Because the maximum operating temperature was 70 °C and the Mach number remained low, the flow was treated as incompressible for the purpose of design comparison. The numerical model solved the Reynolds-averaged conservation equations of mass, momentum and energy under steady-state conditions. Turbulence effects were represented through an effective viscosity and a two-equation turbulence closure. The steady RANS conservation equations used for the CFD model were written in the standard conservative form commonly adopted in CFD-based drying simulations [3] and in SolidWorks Flow Simulation technical documentation [26]:

$$\nabla \cdot u = 0 \tag{3}$$

$$\rho(u \cdot \nabla)u = -\nabla p + \nabla \cdot \left[(\mu + \mu_t)\left(\nabla u + \nabla u^T\right)\right] + \rho g \tag{4}$$

$$\rho c_p(u \cdot \nabla T) = \nabla \cdot (k_{eff} \nabla T) + S_h \tag{5}$$

In these equations, $u$ is the time-averaged velocity vector, $\rho$ is the air density, $p$ is the static pressure, $\mu$ is the dynamic viscosity of air, $\mu_t$ is the turbulent eddy viscosity, $g$ is the gravitational acceleration vector, $c_p$ is the specific heat of air at constant pressure, $T$ is the air temperature, $k_{\text{eff}}$ is the effective thermal conductivity, and $S_h$ is the volumetric heat source associated with the electrical resistances. Eq. (3) represents conservation of mass for an incompressible flow. Eq. (4) expresses the momentum balance, including pressure forces, viscous and turbulent diffusion, and body force effects. Eq. (5) represents conservation of thermal energy, where the heat released by the electrical resistances is transferred to the airflow inside the heating chamber.

For turbulence closure, the shear-stress transport $k-\omega$ model was considered appropriate for reporting the numerical methodology because it combines the near-wall sensitivity of the $k-\omega$ formulation with the free-stream robustness of the $k-\varepsilon$ model. This is relevant for the present dryer because the airflow passes through abrupt expansions, contractions, curved sections, a deflector, spiral heaters and the conical reactor, all of which may generate separation, recirculation and strong velocity gradients. The shear-stress transport (SST) $k-\omega$ turbulence model equations were reported according to Menter's formulation [27] and the SolidWorks Flow Simulation technical reference [26]:

$$\frac{\partial(\rho k)}{\partial t} + \nabla \cdot (\rho k u) = \nabla \cdot [(\mu + \sigma_k \mu_t) \nabla k] + P_k - \beta^* \rho k \omega \tag{6}$$

$$\frac{\partial(\rho \omega)}{\partial t} + \nabla \cdot (\rho \omega u) = \nabla \cdot [(\mu + \sigma_\omega \mu_t) \nabla \omega] + \alpha \frac{\omega}{k} P_k - \beta \rho \omega^2 + 2(1 - F_1) \rho \sigma_{\omega_2} \frac{1}{\omega} \nabla k \cdot \nabla \omega \tag{7}$$

$$\mu_t = \frac{\rho a_1 k}{ax\,(a_1 \omega, S F_2)} \tag{8}$$

In Eqs. (6)–(8), $k$ is the turbulent kinetic energy, $\omega$ is the specific turbulence dissipation rate, $P_k$ is the production of turbulent kinetic energy due to mean velocity gradients, $\beta^* \rho k \omega$ is the dissipation term in the $k$-equation, and $\alpha$, $\beta$, $\beta^*$, $\sigma_k$, $\sigma_\omega$, $\sigma_{\omega 2}$, and $a_1$ are empirical closure coefficients of the SST formulation. The functions $F_1$ and $F_2$ are blending functions that activate the $k-\omega$ behavior near solid walls and gradually transition toward a $k-\varepsilon$-type behavior away from the wall. The scalar $S$ represents the invariant measure of the strain-rate tensor and is used to limit the turbulent eddy viscosity in adverse pressure-gradient regions. The final cross-diffusion term in Eq. (7) is one of the features that allows the SST model to blend both turbulence formulations.

### 2.2.2 Computational domain, mesh generation and boundary conditions

The computational domain was defined to reproduce the air path from the blower outlet to the reactor exhaust. The mesh was generated using the automatic meshing tools available in SolidWorks Flow Simulation. This approach is based on a Cartesian finite-volume mesh with local refinements around walls, narrow passages, curvature changes and regions with high flow or thermal gradients. In the present dryer, local refinement is especially relevant near the 2 in inlet and outlet ducts, the conical inlet and outlet of the heating chamber, the flat deflector, the spiral heaters, the elbow, the mesh-support region, the lower conical reactor and the upper exhaust hole. These regions contain abrupt changes in cross-sectional area or flow direction and therefore control the predicted pressure drop, recirculation zones, velocity recovery and outlet temperature distribution.

Table 4 details the boundary conditions used for the problem setup, the inlet was prescribed from the experimental blower characterization. At 60 Hz, the measured outlet velocity was 35.5 m/s and the corresponding volumetric flow rate was 0.0725 $m^3$/s. For the design simulations, the inlet volumetric flow rate was varied from 0.046 to 0.070 $m^3$/s to represent the practical operating range of the blower. The outlet was assigned as a static-pressure opening at atmospheric pressure. All solid surfaces were treated as no-slip walls. The heating chamber was considered thermally insulated at the design stage, consistent with the proposed use of refractory and insulation materials around the chamber.

**Table 4.** Boundary conditions and modeling assumptions used in the SolidWorks Flow Simulation cases

| Boundary Conditions and Air Properties | Description and Value |
|---|---|
| Inlet | Velocity or mass-flow inlet based on blower data at selected frequency; maximum measured outlet velocity 35.5 m/s and $Q = 0.0725$ $m^3$/s at 60 Hz |
| Outlet | Gauge pressure $p = 0$ kPa |
| Walls | No-slip wall condition |
| Heating chamber wall | Adiabatic assumption for external walls (perfect insulation) |
| Electrical heaters | Total heat demand 3.40 kW distributed in four 900 W resistors = 3.60 kW installed |
| Air properties | Constant pressure ideal gas at approximately 30–70 °C |

The electrical heating elements were represented as internal heat sources distributed over the corresponding resistor geometry. The ideal heating demand was calculated from the airflow rate and the target temperature increase from approximately 30 °C to 70 °C. The installed configuration consisted of four spiral electrical resistances of 900 W each, giving a total installed power of 3.60 kW. This value is slightly higher than the ideal heat demand of 3.40 kW and therefore provides a design margin to compensate for thermal losses and non-ideal heat transfer. Air properties were assigned for the expected operating temperature range. If temperature-dependent properties were activated in the final SolidWorks model, this must be stated explicitly in the final manuscript.

The coffee grains were not modeled as individual moving particles in this design stage. Instead, the simulations focused on the airflow pattern in the empty dryer and at the bed-support region. The mesh-support plane was located 50 mm above the start of the reactor, and the proposed support consisted of a galvanized mesh with square openings of approximately 0.5 mm. This modeling decision is consistent with the objective of comparing geometry-induced airflow behavior before carrying out full drying experiments.

#### 2.2.3 Numerical analysis of the heating chamber design

The heating chamber was designed to allow the airflow delivered by the blower to expand, decelerate, receive heat from the electrical resistances and then recover velocity before entering the reactor. Because the blower draws ambient air through its inlet filter, the air entering the heating chamber corresponds to the surrounding air available in the laboratory. The chamber was located downstream of the blower and upstream of the conical reactor because installing the heating system before the blower would interfere with the blower inlet and could expose the equipment to excessive temperature.

The upstream pipe diameter was kept at 50.8 mm (2 in) because the experimental and numerical observations showed that this diameter preserves a concentrated airflow and a relatively uniform velocity profile before expansion. A heating-chamber diameter of 152.4 mm (6 in) was adopted to accommodate the selected spiral resistances, whose maximum diameter was approximately 130 mm. The chamber was designed with a conical inlet and a conical outlet in order to promote expansion before heating and gradual velocity recovery after heating. The general design concepts evaluated for the heating chamber are shown in Figure 6.

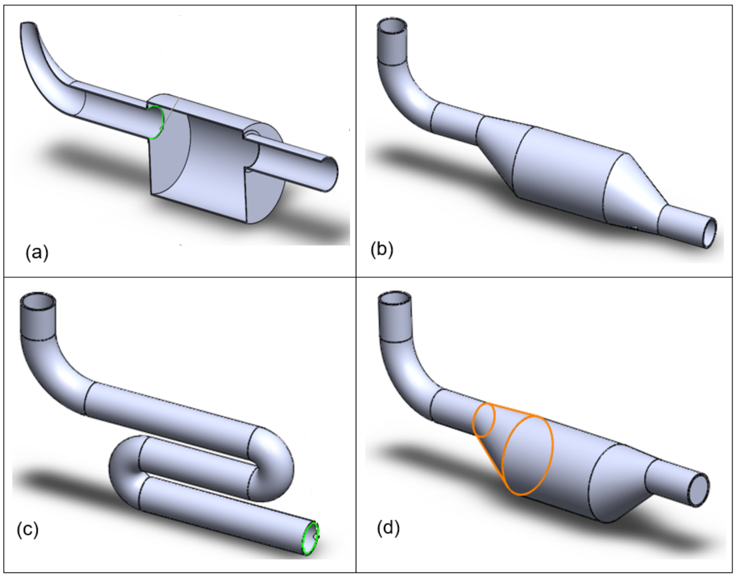


**Figure 6.** Heating-chamber concepts evaluated numerically: (a) straight cylindrical chamber; (b) chamber with axially opposed conical sections; (c) compact coil-type chamber; (d) chamber with conical inlet and outlet sections

Design 1 consisted of a fully cylindrical chamber with inlet and outlet pipes of the same diameter, equal to 25.4 mm. This configuration did not promote adequate airflow expansion and therefore was considered unfavorable. Design 2 introduced conical sections to guide expansion and contraction, but the simulations indicated that the main jet could still cross the chamber without sufficient mixing. Design 3 used a narrower coil-like path to avoid oversizing, but this option increased geometric complexity and was less convenient for construction. Design 4 combined a cylindrical central chamber with conical inlet and outlet sections. This configuration was selected as the base geometry because it allowed the airflow to expand in the heating zone and then recover part of its velocity before entering the elbow and reactor.

A deflector was then incorporated into the heating chamber to disturb the main jet, increase mixing and improve heat transfer between the spiral resistances and the airflow. The simulations showed that placing the deflector near the chamber inlet was more effective than placing it near the outlet, because the inlet position disrupts the high-momentum jet before it crosses the chamber. A flat deflector was finally preferred because it produced the desired flow disturbance while remaining simpler and less expensive to manufacture than a vane-type deflector.

After leaving the heating chamber, the air changes direction through a curved elbow before entering the reactor. The elbow was designed with a curvature radius of approximately 100 mm to reduce abrupt separation and avoid the severe recirculation that would occur in a sharp 90° corner. This component is shown in Figure 7. The elbow was not treated as an isolated design contribution; rather, it was included as part of the complete airflow path to evaluate how the heated air enters the lower section of the conical reactor.

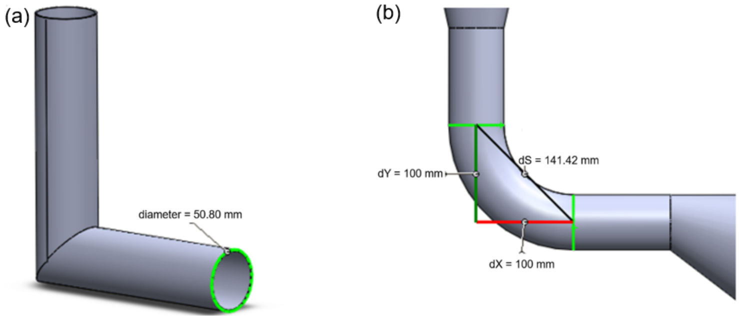


**Figure 7.** Curved elbow used to redirect the heated airflow from the horizontal heating chamber to the vertical reactor inlet

2.2.4 Numerical analysis of the electrical-resistance arrangement geometry

The resistor arrangement was evaluated numerically because the location and shape of the heaters affect both temperature uniformity and pressure losses. The electrical heating requirement was estimated from a steady-flow sensible heat balance [28, 29]:

$$P_e = \rho Q c_p (T_f - T_0) \tag{9}$$

The design form was written as:

$$P_{e,\text{ design}} = S_f \rho Q c_p (T_f - T_0) \tag{10}$$

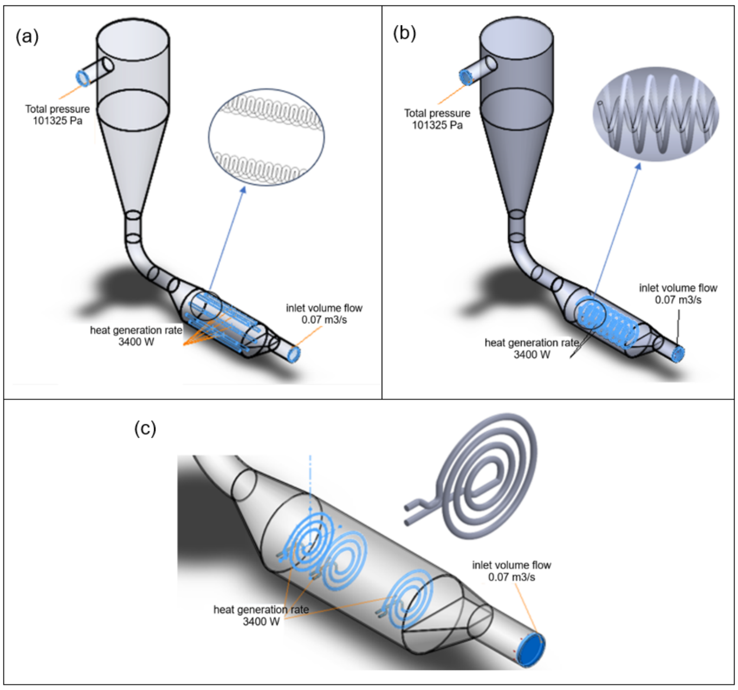


**Figure 8.** Electrical-resistance arrangements evaluated in the heating chamber: (a) wall-mounted longitudinal resistors; (b) central tubular resistors; (c) internal spiral resistors

In Eq. (10), $P_{e,\text{ design}}$ is the design electrical power required to heat the airflow, $S_f$ is the design or safety factor used to compensate for thermal losses and non-ideal heat transfer, $\rho$ is the air density, $Q$ is the inlet volumetric flow rate, $C_p$ is the specific heat of air, $T_f$ is the target outlet air temperature and $T_0$ is the inlet air temperature. For the present design, the inlet temperature measured after the blower was approximately 30 °C, and the target outlet temperature was 70 °C. Using the maximum blower operating condition, the ideal heating demand was approximately 3.40 kW. Therefore, four spiral resistances of 900 W were selected, providing 3.60 kW of installed power. Thus, the available heater capacity provides an approximate design factor of 3.60/3.40 = 1.06. This factor accounts only for the installed electrical margin.

Three main heater arrangements were compared and it can be seen in Figure 8. The first option placed resistances along the lateral contour of the chamber. This configuration produced local heating close to the chamber wall, while the central airflow remained comparatively cooler; therefore, a considerable part of the heat would be transferred to the structure rather than to the useful airflow. The second option placed tubular resistances in the center of the chamber. This improved the interaction with the airflow but increased manufacturing and installation complexity. The third option used spiral resistances placed inside the chamber. The simulations showed that spiral resistances do not block the flow path as severely and provide a better compromise between heat transfer, manufacturability and velocity preservation.

A non-uniform spacing of three spiral resistances initially produced temperature differences among streamlines because slower streams received more heat than faster streams. Consequently, the final configuration used four uniformly spaced spiral resistances distributed along the chamber. This arrangement was selected because it better distributed the 3.60 kW installed power, improved the thermal field at the chamber outlet and avoided excessive flow obstruction. The first resistance was located downstream of the deflector, allowing the disturbed airflow to interact with the heating elements after the jet had begun to expand.

## 3 Results and Discussion

### 3.1 Reactor Design

#### 3.1.1 Cylindrical reactor fluidization tests

According to Table 2, the volumetric flow rate at 60 Hz is 0.0725 $m^3/s$. Based on the cross sectional area around the digital anemometer, this flow rate corresponds to a theoretical bulk velocity of near to 2 m/s. However, the experimentally measured velocity was 1.6 m/s, indicating a deviation from the ideal value. This discrepancy suggests that local flow phenomena, such as area expansion, may be affecting the velocity distribution. Therefore, a numerical simulation was conducted using SolidWorks to investigate the airflow behavior under these geometric conditions (see Figure 9).

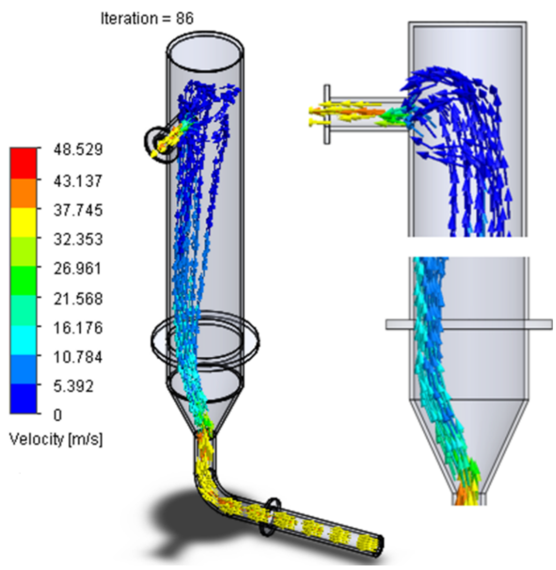


**Figure 9.** Simulated airflow streamlines in the existing cylindrical prototype, showing preferential flow attachment near the reactor wall

As observed in Figure 9, the airflow predominantly moves away from the center. The blower supplies air at approximately 35 m/s, which decreases to 23 m/s at the distributor inlet and further drops to 5 m/s at the top of the reactor. The flow remains largely attached to the side surface of the reactor, failing to generate the expected area expansion. This explains the discrepancy between the theoretical prediction and the value measured by the velocity sensor.

Since the lateral side where the flow predominantly occurred could not be identified, the blower was kept running, and the velocity was subsequently measured at four points on the prototype bed, as shown in Figure 10. The measured velocities at these points exhibit notable variation, indicating that increasing the flow cross section leads to a non uniform velocity distribution across the bed. Consequently, fluidization occurs unevenly: some particles remain non fluidized even when their diameter is relatively large.

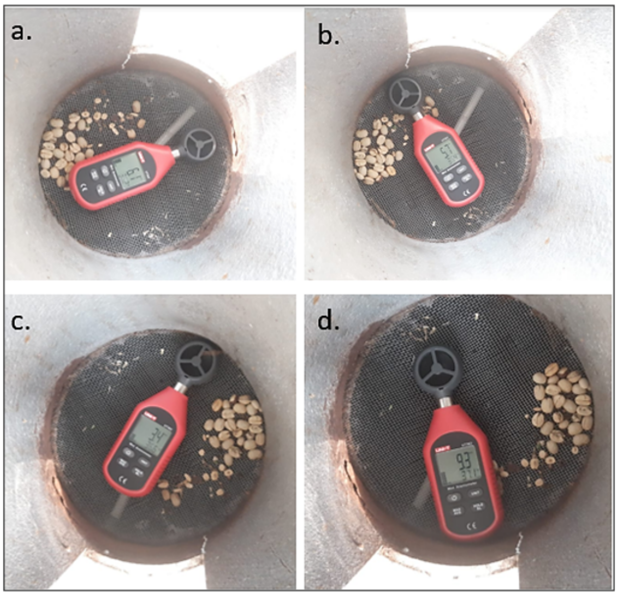


**Figure 10.** Experimental velocity-measurement points on the cylindrical bed section used to assess flow non-uniformity

A test was conducted to verify the aforementioned hypothesis using 500 g of parchment coffee (see Figure 11). The minimum fluidization velocity required to fluidize this specific mass of coffee was calculated using Eq. (1), yielding a value of 19.53 m/s. This result determined the design of a bed with an approximate diameter of 50.8 mm (2 in). This diameter matches the pipe diameter for which a maximum velocity of 35.5 m/s was observed at 60 Hz (see Table 1). The results of the fluidization tests performed with 500 g of coffee are summarized in Table 2. Although the airflow exerted a force on the coffee beans across multiple regions of the lateral surface, it was observed that the area directly in front of the acrylic visor experienced a more pronounced pushing effect.


**Figure 11.** Fluidization behavior of 500 g of parchment coffee in the cylindrical reactor, showing localized rather than uniform grain motion

A subsequent experiment was conducted at 60 Hz using 3 kg of coffee. The results, presented in Figure 12, show a modest increase in observable fluidization compared to the 500 g trial. This improvement may be attributed to the relatively wide surface area of the bed, which prevents the coffee beans from becoming tightly packed. As a result, adequate interstitial spaces are maintained, facilitating airflow and promoting fluidization. Nevertheless, it was observed that not all grains reached a fully fluidized state.

The cylindrical tests therefore indicate that the observed limitation is primarily geometric rather than purely energetic. Although the blower provided sufficient velocity at the pipe outlet, the sudden expansion into the cylindrical chamber reduced the average velocity and caused the jet to follow a preferential path along the lateral wall. This behavior is important because it means that increasing the blower frequency alone would not necessarily solve the problem; a higher flow rate could intensify the local jet while leaving low-velocity regions within the bed. Consequently, the design criterion was shifted from simply increasing air supply to reshaping the lower reactor region so that the available momentum could be used more effectively for grain lifting and circulation.


**Figure 12.** Fluidization behavior of 3 kg of parchment coffee in the cylindrical reactor at 60 Hz

3.1.2 Selection of the distributor geometry

In the initial stage of the experiment, a distributor with a limited number of boreholes was simulated (see Figure 13), which differs markedly in geometry from a mesh type distributor. The results indicate that the air stream was effectively dispersed; however, the outcome is not optimal, as the maximum recorded velocity was only 25 m/s.

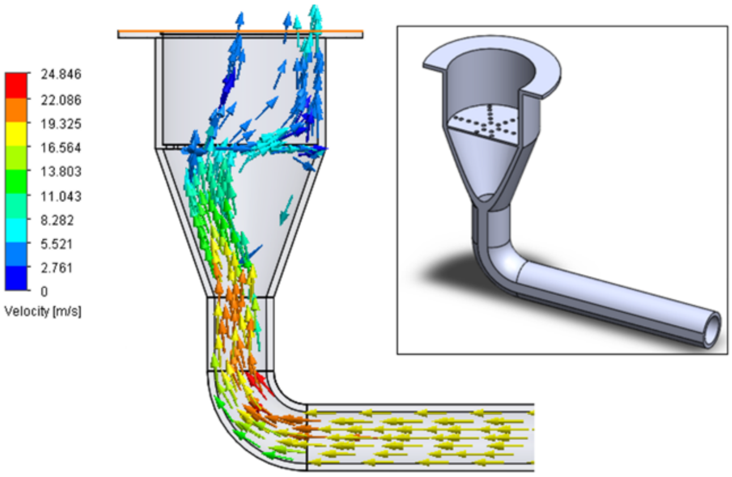


**Figure 13.** Simulated airflow distribution using the first perforated distributor configuration

A second distributor was developed, featuring perforations arranged in a circular pattern (see Figure 14). This design produced superior results, demonstrating a more uniform distribution of the air currents entering the reactor. The airflow velocity fluctuates around 7 m/s, which remains below the minimum fluidization velocity of 19 m/s. This deficiency is attributed to reflux occurring upstream of the distributor.

To prevent this backflow, the airflow must not remain attached to the reactor wall. Accordingly, a perforated plate was placed at the outlet of the pipe elbow (see Figure 15). This configuration increased the flow velocity due to the sudden reduction in cross sectional area. Moreover, the air stream no longer adhered to the reactor wall, and velocities of approximately 13 m/s were observed as the air passed through the distributor.

In the subsequent simulation, the distributor was removed while the perforated plate was retained at the outlet of the pipe elbow (see Figure 16). It is worth noting that, in the actual prototype to be constructed, the distributor will be replaced by a very fine mesh similar to that shown in Figure 15 to retain the coffee beans during drying. The simulation results show an almost vertically oriented airflow with a velocity of 37 m/s. This configuration would enable greater fluidization in the central region of the bed, whereas the beans located in the peripheral area would remain stationary.

The simulation results indicate that a cylindrical reactor with a diameter of 210 mm is unlikely to achieve fluidization of a 5 kg coffee bed. Moreover, the observed tendency of the airflow to remain attached to the reactor wall suggests that a conical reactor geometry may provide a more effective design for promoting uniform fluidization.

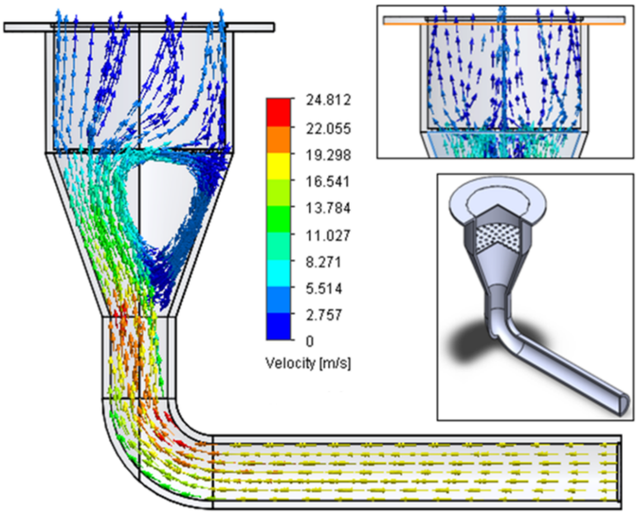


**Figure 14.** Simulated airflow distribution using the second distributor with circularly arranged perforations

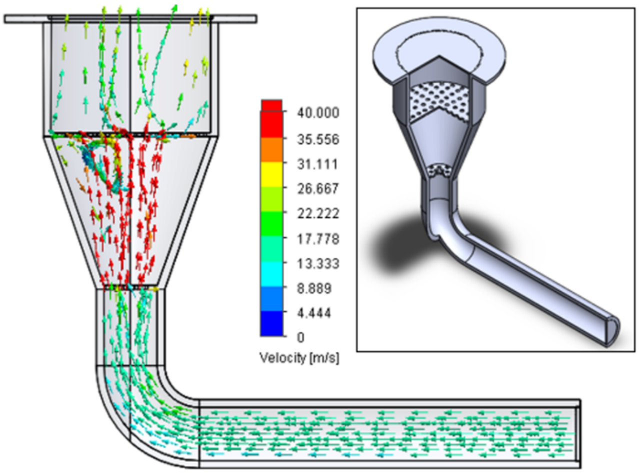


**Figure 15.** Simulated airflow distribution using the second distributor and a perforated plate at the elbow outlet

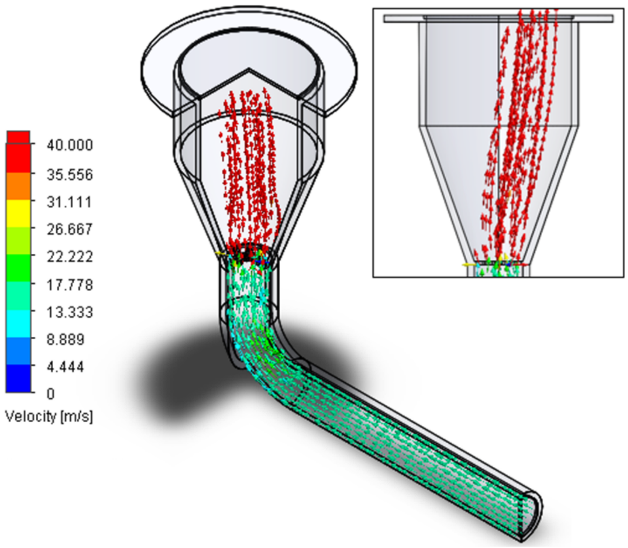


**Figure 16.** Simulated airflow field using only a perforated plate at the elbow outlet, showing a more vertical jet entering the bed region

The distributor simulations also show that a highly restrictive distributor can improve dispersion but may reduce the useful velocity below the level required for fluidization. In contrast, a less restrictive mesh or perforated support preserves more of the inlet momentum but requires an appropriate reactor geometry to avoid a central jet and peripheral stagnation. For this reason, the final configuration did not rely on a distributor as the only corrective element. Instead, the mesh-support region and the conical reactor were treated as complementary components: the mesh retains the coffee grains, while the conical geometry redirects the bed motion and reduces the effective area at the lower section.

### 3.1.3 Conical-reactor screening and final selection

Regarding the simulations of airflow behavior in a conical reactor, an initial geometry with an opening angle of 25° was designed (see Figure 17). The simulation results, shown in Figure 18, indicate that the airflow adheres to the side wall, with final velocities ranging from 37 m/s to 16 m/s.

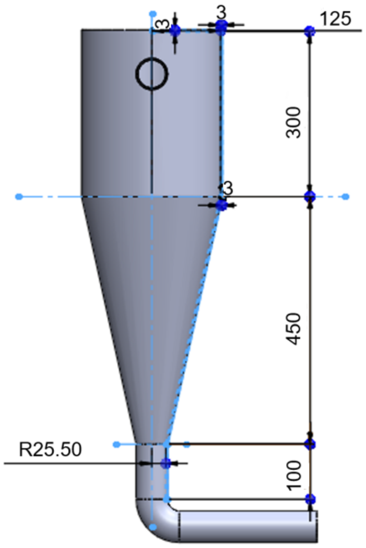


**Figure 17.** Geometry of the 25° conical reactor evaluated in the numerical simulations

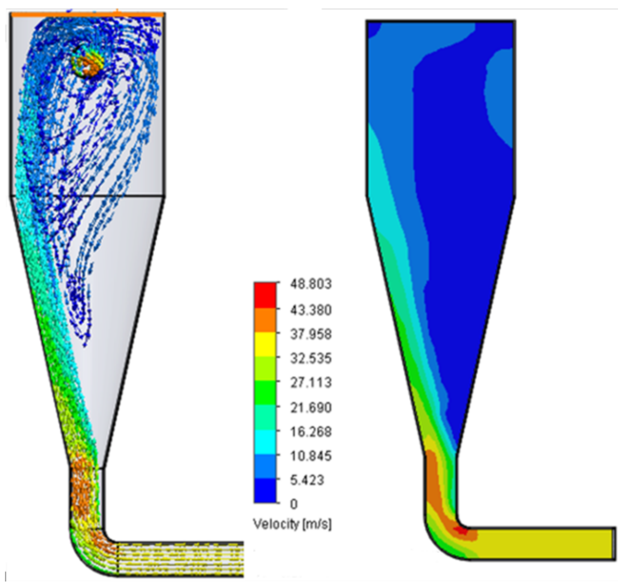


**Figure 18.** Simulated airflow behavior in the 25° conical reactor, showing high-velocity regions available for grain lifting

In the aforementioned figure, a velocity map is presented on a raised plane. The objective is to direct the already fluidized grains toward the blue region (right side) so that they return to the reactor inlet. In the subsequent design, the reactor opening angle was increased to 30° (see Figure 19). Compared to the 25° reactor, this configuration produced a broader zone where the velocity reached 16 m/s in the velocity map. However, the region corresponding to 27 m/s remained similar in extent, generating a greater thrust on the grains (see Figure 20). Finally, as observed in the simulation of the 20° conical reactor, the airflow tends to become vertically aligned. The near zero velocity streams no longer generate backflow and are drawn toward the reactor inlet, entrained by the higher thrust streams (see Figure 21).

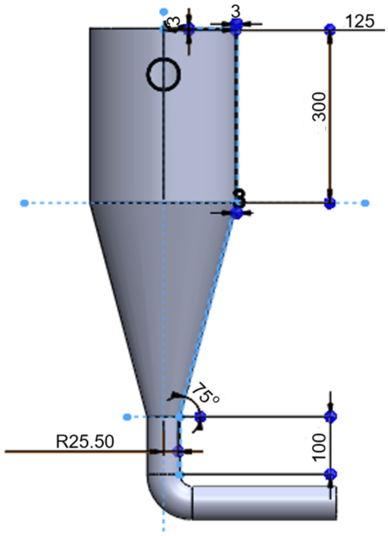


**Figure 19.** Geometry of the 30° conical reactor evaluated in the numerical simulations

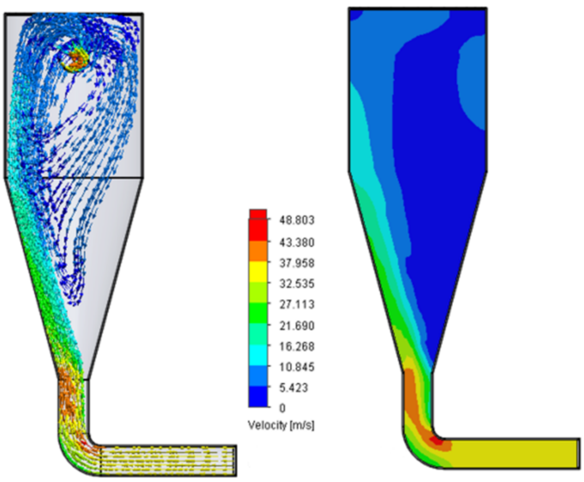


**Figure 20.** Simulated airflow behavior in the 30° conical reactor

The simulation results indicate that the conical reactor geometry offers distinct advantages over the cylindrical design. Among all configurations evaluated, the 25° opening angle was identified as the optimal choice for the intended application, based on the resulting flow velocities and available internal space. In the experimental tests conducted with the prototype, the cone that enabled successful fluidization also featured an opening of approximately 25°. In the study by Das et al. [12], reactors with opening angles of 5° and 10° were compared using a 2.5 kg coffee mass, and the larger angle demonstrated superior fluidization performance. Conversely, the 10° conical reactor initially employed in the prototype experiments (see Figure 5) led to grain agglomeration, preventing the airflow from overcoming the accumulated weight of the bed.

The volume occupied by 5 kg of parchment coffee is 0.0072 $m^3$. For a conical reactor with an opening angle of 25° and a base diameter not exceeding 50.8 mm (2 in), the required height must be at least 440 mm. Experimental observations using the prototype revealed that grains could be visually detected up to 300 mm above the static bed volume. Therefore, a cylindrical extension was added above the conical section to provide sufficient freeboard for fluidization and to prevent grain damage from impact against the upper surface.

The conical-reactor screening confirmed that reactor geometry, rather than blower capacity alone, controlled the achievable bed motion. When the existing distributor was used with a provisional conical structure, the airflow still tended to follow the lateral wall; however, the sloped walls redirected grains from weakly aerated regions toward the lower high-velocity zone. The narrow conical structure was unsuitable for the 5 kg batch because the coffee mass became compressed and the air could not lift the bed. In contrast, the wider conical structure, close to a 25° opening angle, produced the expected circulation pattern, with grains rising in the high-velocity zone and returning through lower-velocity regions. Therefore, the 25° conical reactor was retained as the basis for the final design and for the subsequent CFD comparison with the 20° and 30° alternatives.

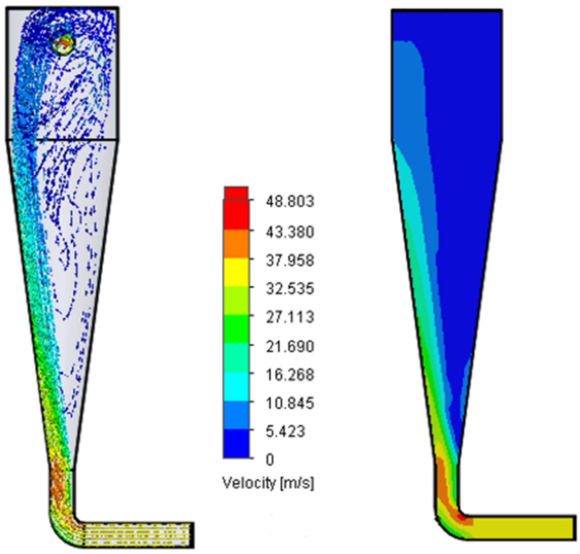


**Figure 21.** Simulated airflow behavior in the 20° conical reactor

### 3.2 Heating Chamber Design

3.2.1 Selection of the heating chamber geometry

A fully cylindrical chamber with the inlet and outlet positioned at the same height (see Figure 22) prevents the airflow from expanding, making this configuration unsuitable for the intended application.

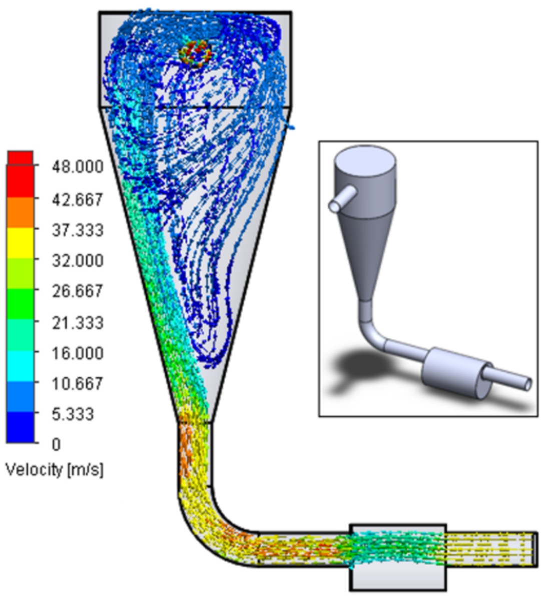


**Figure 22.** Simulated airflow behavior in a fully cylindrical heating chamber with aligned inlet and outlet pipes

Figure 23 illustrates a configuration where the air inlet and outlet of the chamber are located at different heights. In this arrangement, low velocity streams detach from the main flow, leading to an increase in localized thrust and the formation of recirculation zones. However, overall airflow expansion remains suppressed.

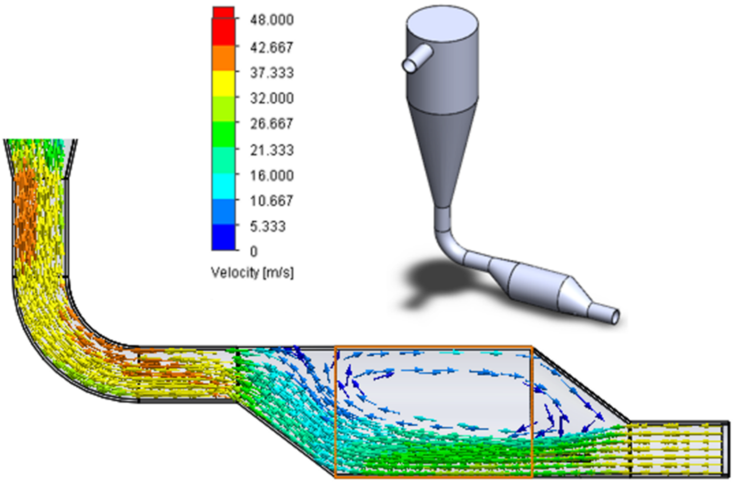


**Figure 23.** Simulated airflow behavior in a heating chamber with axially opposed truncated-cone sections

By placing two truncated cones vertically opposite each other (see Figure 24), a phenomenon occurs in which the higher thrust air stream enters the reactor, while the lower thrust streams generate backflow in the empty region of the chamber. This outcome prompted the addition of baffles, which serve as obstacles to induce turbulence.

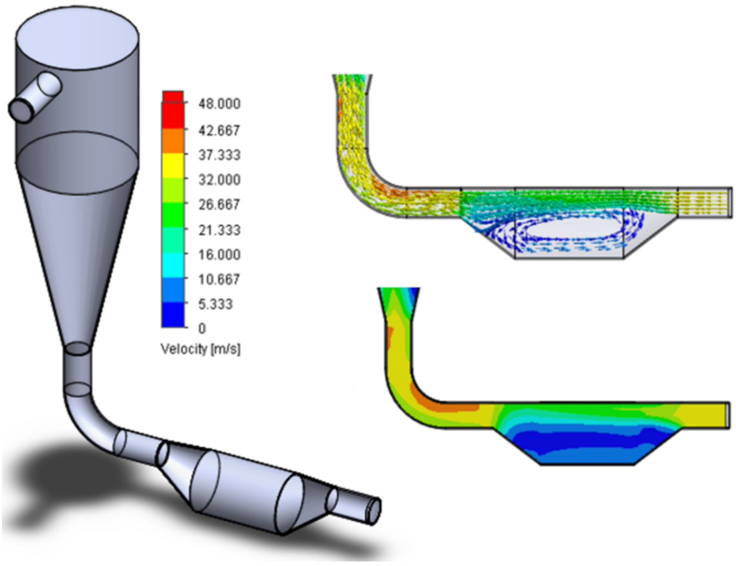


**Figure 24.** Simulated airflow behavior in a heating chamber with vertically opposed truncated-cone sections

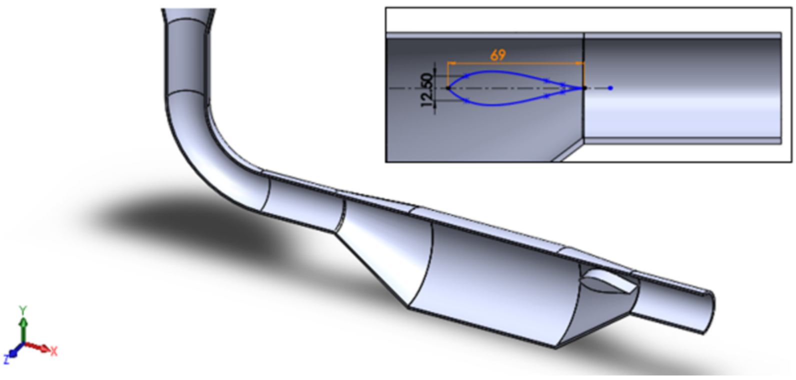


**Figure 25.** Horizontal vane inserted as an internal deflector in the heating chamber

The obstacle should be placed at the inlet of the chamber, since positioning it at the outlet would induce backflow and hinder the recovery of air velocity after expansion. The first deflector tested was a horizontal vane (see Figure 25), which forces the airflow to travel over its surface and then recombine downstream. Subsequently, the deflector was installed at an inclined angle (see Figure 26). This configuration resulted in increased turbulence, suppression of backflow, and effective velocity recovery.

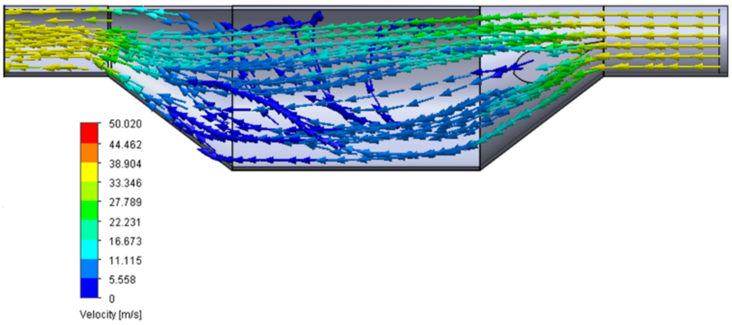


**Figure 26.** Simulated airflow behavior in the heating chamber using an inclined vane deflector

In order to reduce the expenses related to the fabrication and assembly of bladed deflectors, a geometrically simpler deflector was considered for comparison. As shown in Figure 27, this design likewise promotes increased turbulence (see Figure 28).

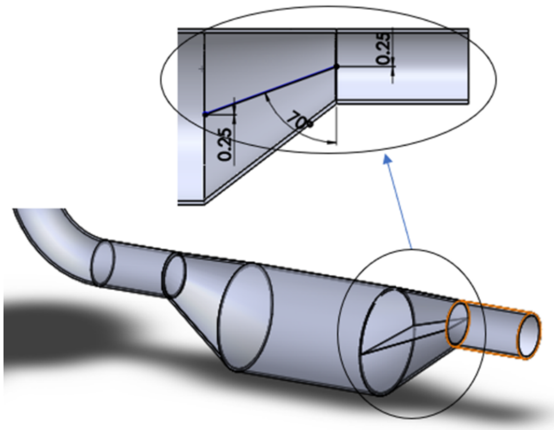


**Figure 27.** Flat baffle inserted near the inlet region of the heating chamber

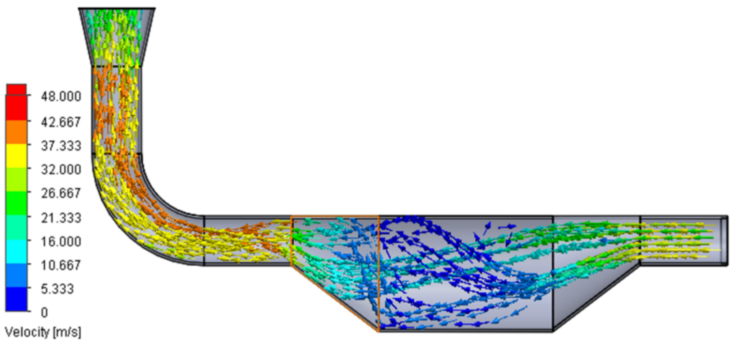


**Figure 28.** Simulated airflow behavior in the heating chamber using the flat baffle

A comparison of the simulated airflow behavior for the different baffle designs revealed that the flat baffle closely replicates the flow characteristics observed in Figure 26, making it a cost effective alternative. Furthermore, the influence of drag within the chamber on the turbulence of the airflow must also be taken into account.

From a design perspective, the baffle does not act only as a turbulence generator; it also increases the residence time of the air in the heating chamber. This is relevant because the chamber must both transfer heat and deliver the air to the reactor without excessive loss of velocity. The flat baffle was therefore selected as a practical compromise between thermal mixing, aerodynamic simplicity and manufacturability. Its geometry is easier to fabricate than a blade-type deflector and is less likely to increase maintenance complexity in a small-scale prototype.

### 3.3 Selection of the Geometry of Electrical Resistors

The required heating power for the air is calculated to be 3.40 kW. The air enters the chamber at 30 °C, and the target is to raise its temperature to a maximum of 70 °C.

#### 3.3.1 Chamber contour resistors

The initial design proposal places eight electrical resistors along the lateral surface of the chamber (see Figure 29). Simulation results indicate that the temperature rises to approximately 80 °C in the regions near the resistors, while the central zone remains comparatively cool. Consequently, this heater arrangement is inadvisable, as most of the heat would be transferred to the structural components of the dryer rather than to the airflow.

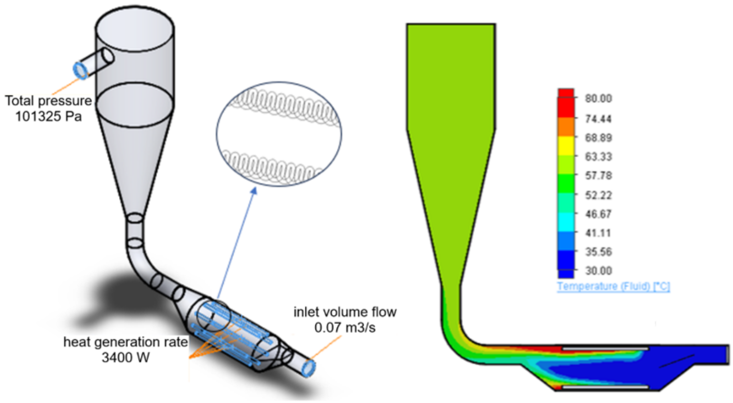


**Figure 29.** Air-temperature field obtained with wall-mounted electrical resistors in the heating chamber

#### 3.3.2 Tube-shaped resistors in the center of the chamber

The subsequent design features two tubular resistors placed at the center of the chamber, with a combined heating capacity of 3.4 kW (see Figure 30). The results show a temperature increase along the heaters, although only one zone within the chamber reaches values approaching 80 °C. While the reactor temperature approaches 63 °C, the configuration and installation of such an arrangement would be inherently complex.

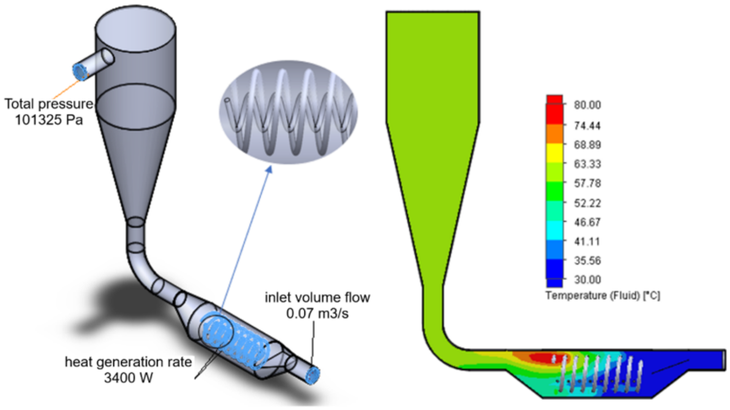


**Figure 30.** Air-temperature field obtained with tubular electrical resistors located near the chamber centerline

#### 3.3.3 Non-uniformly spaced spiral resistors

In the next design, spiral resistors were considered. Initially, three resistors were proposed: the first placed in front of the deflector to promote air expansion, and the other two located at the far end of the chamber, where the expanded fluid would reach them. As shown in Figure 31 (for the spiral configuration), the air temperature increases after passing through the two downstream resistors, reaching significantly higher values in a specific region of the reactor. This observed behavior may initially appear inconsistent with expectations. However, Figure 32 reveals that air streams at 70 °C flow along the side surface, while streams at 46 °C pass through the center. This phenomenon is attributed to the non uniform streamline pattern downstream of the deflector. The slower streamlines experience greater heat transfer from the resistors, resulting in a more pronounced temperature rise compared to the faster streamlines.

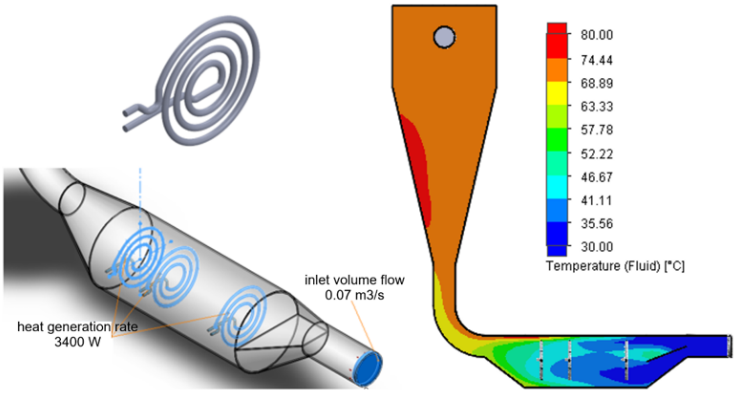


**Figure 31.** Air-temperature field obtained with non-uniformly spaced spiral electrical resistors

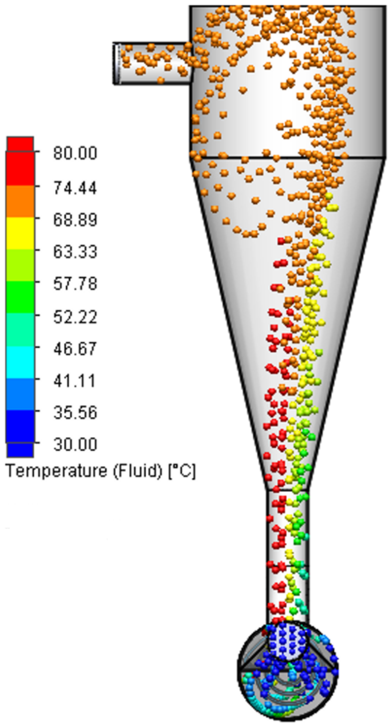


**Figure 32.** Particle-path representation colored by air temperature, showing non-uniform heating among streamlines

### 3.3.4 Uniformly spaced spiral resistors

Subsequently, a simulation of the dryer was performed using four electrical resistors in an attempt to achieve a uniform temperature distribution within the fluid. The simulation results indicate that some streams still exhibit higher temperatures than others. Nevertheless, the chamber length is sufficient to adequately heat the air (see Figures 33 and 34). The spiral heaters do not cause a velocity loss due to their open cross section, making them the optimal choice for the intended application. It can be concluded that using four heaters instead of three to supply the required thermal power (3400 W) provides a net benefit in terms of heating uniformity. Moreover, four heaters are preferable because each of these units can deliver a maximum of 900 W, making the configuration both feasible and effective.

The final selection of four uniformly spaced spiral resistors should therefore be interpreted as both a thermal and hydraulic decision. Thermally, the four-resistor configuration distributes the installed 3.60 kW power more evenly along the chamber length. Hydraulically, the spiral geometry leaves an open central region through which the airflow can pass, reducing the risk of excessive pressure drop. This explains why the uniformly spaced spiral arrangement was preferred over wall-mounted resistors, which heated the structure more than the central air stream, and over tubular resistors, which were more complex to install.

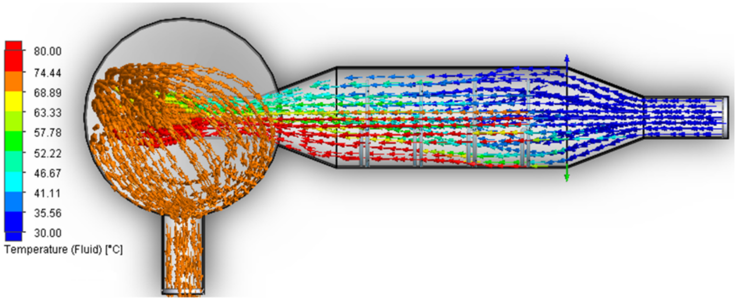


**Figure 33.** Plan view of airflow streamlines colored by temperature for the uniformly spaced spiral-resistor configuration

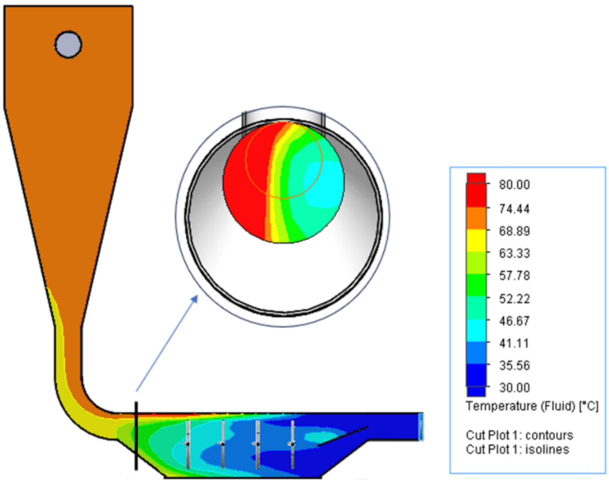


**Figure 34.** Vertical mid-plane temperature field near the heating-chamber outlet and elbow inlet for the uniformly spaced spiral-resistor configuration

### 3.4 Presentation and Simulation of the Final Design

The final design of the fluidized bed dryer, shown in Figure 35, was defined based on the simulation results and theoretical considerations.

These prototype exhibits the following characteristics:

(a) Connecting pipe (blower to heating chamber): Diameter 50.8 mm (2 in), length 150 mm (hereafter referred to as "pipe A").

(b) Heating chamber: Composed of two truncated cones placed at the inlet and outlet. Each cone has a length of 100 mm, a small base diameter of 50.8 mm (2 in), and a large base diameter of 152.4 mm (6 in). A diameter of 127 mm (5 in) was initially considered because simulations showed superior turbulence behavior at that size; however, the air temperature at the outlet did not reach 70 °C, and the available spiral heaters have a diameter of 130 mm.

(c) Pipe elbow (connecting heating chamber to conical reactor): Diameter 50.8 mm (2 in), bending radius 100 mm. As with the prototype, this component must be sent for fabrication.

(d) Conical reactor: Opening angle 25°, large base diameter (at the top) 250 mm. With these dimensions and a height of 440 mm, the internal volume is sufficient to hold up to 5 kg of parchment coffee.

(e) Cylindrical extension (lid): Added above the conical section to provide sufficient freeboard for fluidization, allowing the beans to move freely. The lid has a height of 300 mm and contains a 50.8 mm (2 in) diameter outlet for humid air, to which a 100 mm long tube is connected.

(f) Heating elements: Four spiral electrical resistors, each with a maximum diameter of 130 mm and a rated power of 900 W (adjustable). They are arranged equidistantly at 70 mm spacing within the chamber. The first resistor is located 20 mm downstream of the deflector.

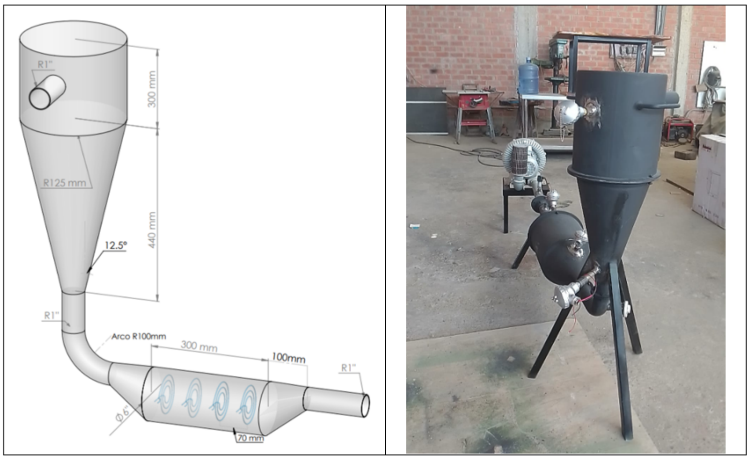


**Figure 35.** Final fluidized-bed dryer (FBD) design: (a) three-dimensional assembly; (b) constructed prototype

As shown in Figure 36, the airflow within the entire prototype was simulated. The support bed for the coffee beans is located at a height of 50 mm above the inlet of the conical reactor; this arrangement was determined based on findings from the experimental phase.

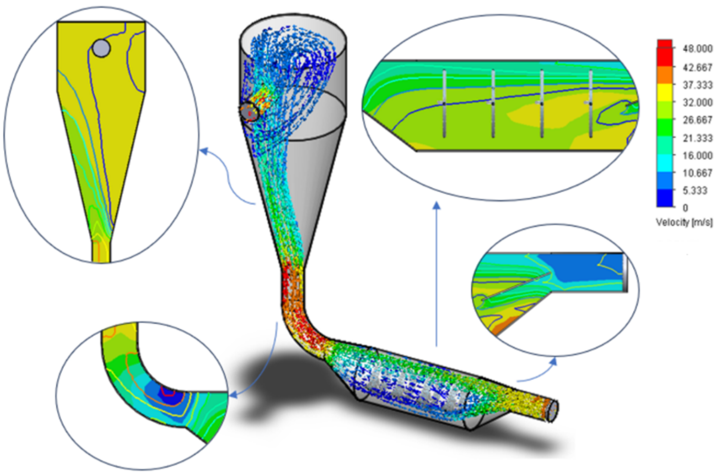


**Figure 36.** Simulated airflow path through the complete proposed dryer assembly

Figure 37 presents the velocity profile for the aforementioned region. The support bed will be fabricated from a galvanized mesh with square openings of 0.5 mm per side. The wire diameter is relatively small, offering minimal resistance to the airflow.

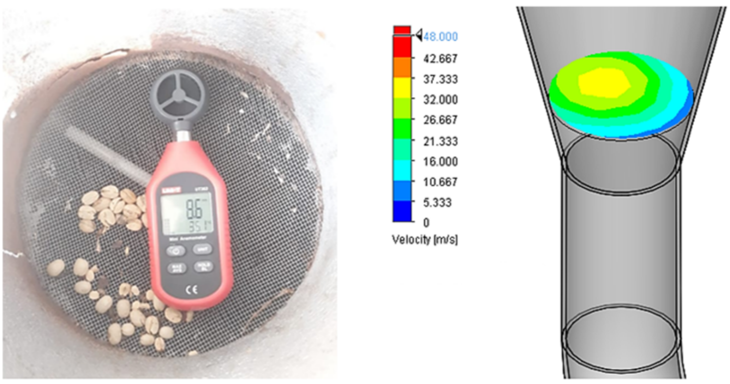


**Figure 37.** Velocity profile at the mesh-support/bed region located 50 mm above the conical reactor inlet

It is instructive to examine the flow behavior within the reactor, given its relatively large cross section compared to the upstream pipes. Figure 38 presents a side view of the flow field using sectional cutouts. In regions where the simulation shows no vectors or a blue color, the air velocity is low. Distinct fluidization zones can be identified. The air stream in the central region of the reactor exhibits a velocity gradient that decreases with vertical height, a consequence of the airflow's tendency to adhere to the reactor wall. Near the wall, the air velocity ranges from 16 to 25 m/s.

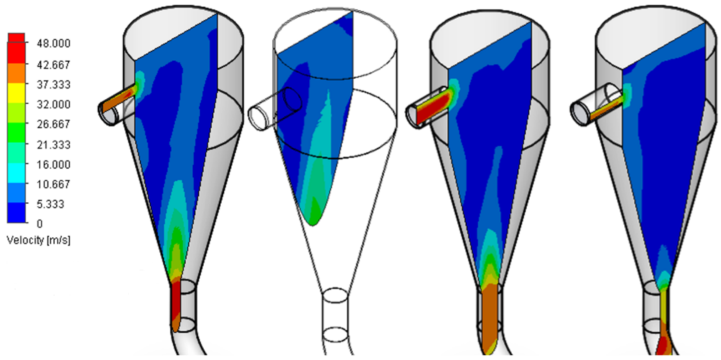


**Figure 38.** Longitudinal velocity contours inside the conical reactor, showing high- and low-velocity fluidization zones

### 3.5 General Discussion

The experimental observations and numerical simulations indicate that the original cylindrical prototype was limited mainly by airflow distribution rather than by blower capacity. At 60 Hz, the blower delivered 35.5 m/s and 0.0725 $m^3$/s at the pipe outlet; however, the sudden expansion into the cylindrical reactor generated a non-uniform velocity field. The jet tended to attach to one side of the wall, producing local high-velocity regions while leaving other areas weakly aerated. This explains the partial fluidization observed with 500 g and 3 kg of parchment coffee and confirms that a larger airflow rate alone would not guarantee uniform bed motion.

This result agrees with general fluidized-bed drying literature, where adequate hydrodynamic control is considered essential to avoid channeling, dead zones, segregation and hot spots [7]. Recent CFD-based studies have also shown that temperature and moisture maldistribution can appear in granular beds when the airflow is not properly distributed [20, 22, 30]. Therefore, the present design problem was not only to provide sufficient air velocity, but also to use the reactor geometry to direct the available momentum into the coffee bed more effectively.

The conical reactor was the main design improvement. By reducing the lower cross-sectional area, the conical section increased the local velocity and promoted a circulation pattern in which coffee grains were lifted in the high-velocity region and returned by gravity through lower-velocity zones. This behavior is consistent with Das et al. [12], who found that conical fluidized-bed configurations improved drying characteristics and energy behavior in paddy drying. Although their product and batch size differed from the present work, the same physical principle applies: conical geometry can improve air-particle interaction by modifying the velocity field and promoting particle motion. The present study extends this logic to parchment coffee and to a target mass of 5 kg.

The heating-chamber results also show that thermal and hydrodynamic design must be considered together. The conical inlet and outlet sections allowed the airflow to expand and then recover velocity, while the flat baffle disrupted the main jet and improved mixing before the air reached the electrical resistors. Similar design reasoning has been reported in dryer studies using internal deflectors to improve the uniformity of the drying-agent distribution and reduce energy losses [23, 31]. In the present dryer, the flat baffle was selected because it improved mixing while remaining easier to manufacture than a vane-type deflector.

The arrangement of the electrical resistances was another critical factor. Wall-mounted resistors concentrated heat near the chamber surface, whereas tubular central resistors increased construction complexity. The final four-resistor spiral configuration provided a better compromise because it distributed the installed 3.60 kW power along the chamber and did not excessively obstruct the flow path. The selected maximum temperature of 70 ℃ gives operational flexibility, although coffee-drying studies suggest that lower operating temperatures around 50 ℃ may be favorable for drying efficiency and quality preservation [4, 16, 18, 25]. Therefore, the prototype should be experimentally operated over a controlled range of temperatures rather than only at the maximum heating condition.

Overall, the proposed design is feasible as a pre-validation prototype for 5 kg parchment-coffee fluidization. Its main contribution is the integration of conical reactor geometry, controlled airflow delivery and electric heating into a compact dryer concept. Nevertheless, the study remains a design-stage analysis. Future work must validate drying curves, pressure drop, energy consumption, final moisture distribution and coffee quality, and could also incorporate advanced CFD-DEM or porous-bed modeling to represent the moving coffee bed more realistically [21].

## 4 Conclusion

This study developed and evaluated a compact conical FBD for small-scale parchment-coffee drying. The experimental screening and numerical simulations showed that the main limitation of the previous cylindrical prototype was not blower capacity but poor airflow distribution. Although the blower delivered up to 35.5 m/s and 0.0725 $m^3$/s at 60 Hz, the sudden expansion into the cylindrical reactor caused the jet to attach to one side of the wall, producing localized high-velocity regions and stagnant zones.

The conical geometry improved the use of the available airflow by concentrating the velocity in the lower section and promoting grain circulation. Tests with provisional cones showed that an excessively narrow cone compressed the 5 kg coffee mass, whereas an opening close to 25° allowed grains to rise in the high-velocity zone and return through lower-velocity regions. The final reactor therefore adopted a 25° conical section, a 50.8 mm lower inlet, an approximately 250 mm upper diameter, a 440 mm conical height, and a 300 mm freeboard section.

The heating chamber was also defined from the design-stage simulations. A 152.4 mm chamber with conical inlet and outlet sections, a flat baffle, and four uniformly spaced 900 W spiral electrical resistors provided a manufacturable configuration for air expansion, mixing, velocity recovery, and heating [32]. The installed 3.60 kW heater capacity gives a 5.9% margin relative to the 3.40 kW ideal requirement for increasing air temperature from approximately 30 °C to 70 °C. Overall, the proposed dryer is technically feasible for 5 kg parchment-coffee fluidization; however, drying kinetics, pressure drop, energy consumption, moisture uniformity, and coffee quality must be validated experimentally in future work.

## Author Contributions

Conceptualization, E.M.O. and R.L.M.O.; methodology, E.M.O. and D.M.A.; validation, D.M.A.; formal analysis, E.M.O. and R.L.M.O.; investigation, R.L.M.O.; resources, N.R.C.; data curation, E.M.O. and A.S.M.; writing—original draft preparation, E.M.O. and A.S.M.; writing—review and editing, E.M.O. and G.L.; visualization, G.L.; supervision, N.R.C.; project administration, R.L.M.O. All authors have read and agreed to the published version of the manuscript.

## Data Availability

The data used to support the research findings are available from the corresponding author upon request.

## Conflicts of Interest

The authors declare no conflicts of interest.

## References


[1] C. Díaz Vargas and M. Carmen Willems, "Línea de base del sector café en el Perú," 2014. https://camcafeperu.com.pe/admin/recursos/publicaciones/Linea-base-del-sector-cafe-en-Peru.pdf

[2] L. A. Segura-Ponce, V. A. Soto-Pardo, and M. F. Guzmán-Meza, "Characterization of apples (Granny Smith) dried in industrial equipment and the relationship with drying mechanisms," *Food Struct.*, vol. 21, p. 100119, 2019. https://doi.org/10.1016/j.foostr.2019.100119

[3] N. Malekjani and S. M. Jafari, "Simulation of food drying processes by computational fluid dynamics (CFD): Recent advances and approaches," *Trends Food Sci. Technol.*, vol. 78, pp. 206–223, 2018. https://doi.org/10.1016/j.tifs.2018.06.006

[4] B. Soeswanto, N. L. E. Wahyuni, and G. Prihandini, "The development of coffee bean drying process technology—A review," in *Proceedings of the 2nd International Seminar of Science and Applied Technology (ISSAT 2021)*, Bandung, Indonesia, 2021, pp. 164–170. https://doi.org/10.2991/aer.k.211106.026

[5] D. A. Asrate and A. N. Ali, "Review on the recent trends of food dryer technologies and optimization methods of drying parameters," *Appl. Food Res.*, vol. 5, no. 1, p. 100927, 2025. https://doi.org/10.1016/j.afres.2025.100927

[6] R. T. Patil and D. M. Kadam, "Hot air drying design: Fluidized bed drying," in *Handbook of Food Process Design*. Wiley, 2012, pp. 542–577. https://doi.org/10.1002/9781444398274.ch20

[7] R. Sivakumar, R. Saravanan, A. Elaya Perumal, and S. Iniyan, "Fluidized bed drying of some agro products—A review," *Renew. Sustain. Energy Rev.*, vol. 61, pp. 280–301, 2016. https://doi.org/10.1016/j.rser.2016.04.014

[8] A. S. Kassem, A. Z. Shokr, A. R. El-Mahdy, A. M. Aboukarima, and E. Y. Hamed, "Comparison of drying characteristics of Thompson seedless grapes using combined microwave oven and hot air drying," *J. Saudi Soc. Agric. Sci.*, vol. 10, no. 1, pp. 33–40, 2011. https://doi.org/10.1016/j.jssas.2010.05.001

[9] T. Nazghelichi, M. H. Kianmehr, and M. Aghbashlo, “Thermodynamic analysis of fluidized bed drying of carrot cubes,” *Energy*, vol. 35, no. 11, pp. 4679–4684, 2010. https://doi.org/10.1016/j.energy.2010.09.036

[10] A. Reyes, A. Mahn, C. Guzmán, and D. Antoniz, “Analysis of the drying of broccoli florets in a fluidized pulsed bed,” *Drying Technol.*, vol. 30, no. 12, pp. 1368–1376, 2012. https://doi.org/10.1080/07373937.2012.686548

[11] S. Soponronnarit, T. Swasdisevi, S. Wetchacama, and W. Wutiwiwatchai, “Fluidized bed drying of soybeans,” *J. Stored Prod. Res.*, vol. 37, no. 2, pp. 133–151, 2001. https://doi.org/10.1016/S0022-474X(00)00015-1

[12] H. J. Das, R. Saikia, and P. Mahanta, “Effects of spiral and cone angles on drying characteristics and energy consumption of fluidized bed paddy dryer,” *Drying Technol.*, vol. 40, no. 4, pp. 852–863, 2022. https://doi.org/10.1080/07373937.2020.1832512

[13] E. M. López Fontal, “Coffee drying on fluidized bed,” *Ing. Investig.*, vol. 26, no. 1, pp. 22–26, 2006. https://doi.org/10.15446/ing.investig.v26n1.14684

[14] D. A. Unigarro Bolaños, “Secado de café arábigo coffea arabica L. de la variedad caturra mediante lecho fluidizado,” diplomathesis, Universidad Técnica del Norte, Imbabura, Ecuador, 2017. https://repositorio.utn.edu.ec/handle/123456789/6154

[15] K. K. Konsil, N. Sazali, K. Kadirgama, W. S. W. Harun, and N. Zainol, “Analysis on the performance of designed fluidized bed dryer for drying coffee beans,” *J. Adv. Res. Appl. Sci. Eng. Technol.*, vol. 31, no. 1, pp. 99–109, 2023. https://doi.org/10.37934/araset.31.1.99109

[16] N. L. E. Wahyuni, B. Soeswanto, G. Prihandini, A. Marlina, E. Widyastuti, M. F. R. Qobus, and R. Rahmawati, “Coffee beans drying using pilot-scaled fluidized bed dryer assisted with zeolite adsorbent,” *Fluida*, vol. 16, no. 2, pp. 99–104, 2023. https://doi.org/10.35313/fluida.v16i2.5337

[17] J. E. Reyes-Chaparro, J. R. Arballo, and L. A. Campañone, “Experimental study of parchment coffee drying using the combined fluidization and microwave process: Analysis of drying curves and thermal imaging,” *J. Food Eng.*, p. 112214, 2024. https://doi.org/10.1016/j.jfoodeng.2024.112214

[18] S. Suherman, H. Hadiyanto, M. A. Asy-Syaqiq, G. A. Ghassani, and M. Ajundasari, “Energy and exergy performance evaluation of a drying coffee beans system using a photovoltaic–direct solar dryer at different drying temperature conditions,” *Int. J. Ambient Energy*, vol. 45, no. 1, p. 2344548, 2024. https://doi.org/10.1080/01430750.2024.2344548

[19] E. Baidhe and C. L. Clementson, “A review of the application of modeling and simulation to drying systems for improved grain and seed quality,” *Comput. Electron. Agric.*, vol. 222, p. 109094, 2024. https://doi.org/10.1016/j.compag.2024.109094

[20] Q. Tu, Z. Ma, and H. Wang, “Investigation of wet particle drying process in a fluidized bed dryer by CFD simulation and experimental measurement,” *Chem. Eng. J.*, vol. 452, p. 139200, 2023. https://doi.org/10.1016/j.cej.2022.139200

[21] M. J. A. de Munck, E. A. J. F. Peters, and J. A. M. Kuipers, “CFD-DEM fluidized bed drying study using a coarse-graining technique,” *Ind. Eng. Chem. Res.*, vol. 62, no. 48, pp. 20 911–20 920, 2023. https://doi.org/10.1021/acs.iecr.3c02960

[22] T. T. H. Tran and K. H. Le, “Computational fluid dynamic simulation of packed bed drying process: Impact of particle properties, drying conditions, and lateral edge heating modes on drying kinetics,” *Int. J. Air-Cond. Refrig.*, vol. 32, no. 1, pp. 1–8, 2024. https://doi.org/10.1007/s44189-024-00047-x

[23] V. N. Arsenoaia, G. R. Roșca, P. Cârlescu, M. Băetu, R. Rațu, I. Veleșcu, and I. Țenu, “Drying process modeling and quality assessments regarding an innovative seed dryer,” *Agriculture*, vol. 13, no. 2, p. 328, 2023. https://doi.org/10.3390/agriculture13020328

[24] Y. Yuwana and S. Syafnil, “Free electricity tandem-twin-hybrid solar-biomass dryer increased the performance of coffee cherry drying,” *Res. Agric. Eng.*, vol. 71, no. 3, pp. 174–187, 2025. https://doi.org/10.17221/98/2024-RAE

[25] N. Nafisah, I. N. Syamsiana, R. I. Putri, W. Kusuma, and A. D. W. Sumari, “Implementation of fuzzy logic control algorithm for temperature control in robusta rotary dryer coffee bean dryer,” *MethodsX*, vol. 12, p. 102580, 2024. https://doi.org/10.1016/j.mex.2024.102580

[26] J. E. Matsson, “An introduction to SOLIDWORKS Flow Simulation 2018,” SolidWorks, 2018. https://static.sdcpublications.com/pdfsample/978-1-63057-163-4-2.pdf

[27] F. R. Menter, “Two-equation eddy-viscosity turbulence models for engineering applications,” *AIAA J.*, vol. 32, no. 8, pp. 1598–1605, 1994. https://doi.org/10.2514/3.12149

[28] Y. A. Çengel and A. J. Ghajar, *Heat and Mass Transfer: Fundamentals and Applications, 6th Ed.* McGraw Hill Education, 2015.

[29] A. A. Freschi, N. R. Caetano, G. A. Santarine, and R. Hessel, “Laser interferometric characterization of a vibrating speaker system,” *Am. J. Phys.*, vol. 71, no. 11, pp. 1121–1126, 2003. https://doi.org/10.1119/1.1586262

[30] S. Dasgupta, M. Das, M. A. Klunk, S. J. S. Xavier, N. R. Caetano, and P. R. Wander, “Copper and chromium removal from synthetic textile wastewater using clay minerals and zeolite through the effect of pH,” *J. Iran. Chem. Soc.*, vol. 18, pp. 3377–3386, 2021. https://doi.org/10.1007/s13738-021-02273-1

[31] M. A. Klunk, Z. Shah, R. V. Conceição, P. R. Wander, S. Dasgupta, and M. Das, “$CO_2$ sequestration by magnesite mineralisation through interaction of Mg-brine and $CO_2$: Integrated laboratory experiments and computerised geochemical modelling,” *Int. J. Environ. Stud.*, vol. 77, no. 3, pp. 492–509, 2020. https://doi.org/10.1080/00207233.2019.1675295

[32] N. R. Caetano, B. P. Da Silva, A. C. Ruoso, A. G. Avila, L. A. O. Rocha, and G. Lorenzini, “Energy recovery based on exhaust gas recirculation and heat regeneration processes applied in a firewood boiler,” *J. Eng. Thermophys.*, vol. 32, pp. 482–501, 2023. https://doi.org/10.1134/S1810232823030062

**Nomenclature**

| | |
|---|---|
| $A$ | Cross-sectional area (m$^2$) |
| $a_1$ | SST $k$-$\omega$ turbulence-model coefficient |
| $c_p$ | Specific heat capacity of air (kJ/(kg·K)) |
| $d, D_e$ | Equivalent diameter of parchment coffee (m or mm) |
| $F_1, F_2$ | SST $k$-$\omega$ blending functions |
| $g$ | Gravitational acceleration (m/s$^2$) |
| $h$ | Specific enthalpy (kJ/kg) |
| $k$ | Turbulent kinetic energy (m$^2$/s$^2$) |
| $k_{\text{eff}}$ | Effective thermal conductivity (W/(m·K)) |
| $m$ | Coffee mass (kg) |
| $p$ | Static pressure (Pa) |
| $P_e$ | Ideal electrical heating power (kW) |
| $P_{e,\text{design}}$ | Electrical heating power including design factor (kW) |
| $P_k$ | Production rate of turbulent kinetic energy (kg/(m·s$^3$)) |
| $Q$ | Volumetric air flow rate (m$^3$/s) |
| $Re$ | Reynolds number |
| $S$ | Strain-rate magnitude used in the SST eddy-viscosity model (1/s) |
| $S_f$ | Safety/design factor for heat losses and control margin |
| $S_h$ | Volumetric heat source (W/m$^3$) |
| $T$ | Air temperature (°C) |
| $T_0, T_f$ | Air temperature at heater inlet and outlet (°C) |
| $u$ | RANS time-averaged velocity vector (m/s) |
| $U_0$ | Superficial gas velocity (m/s) |
| $U_{\text{mf}}$ | Minimum fluidization velocity (m/s) |
| $\beta, \beta^*, \alpha$ | SST $k$-$\omega$ empirical closure coefficients |
| $\varepsilon$ | Bed porosity |
| $\mu$ | Molecular viscosity (Pa·s) |
| $\mu_t$ | Turbulent eddy viscosity (Pa·s) |
| $\rho$ | Air density (kg/m$^3$) |
| $\rho_s$ | Apparent coffee grain density (kg/m$^3$) |
| $\sigma_k, \sigma_\omega, \sigma_{\omega 2}$ | Diffusion coefficients in the SST $k$-$\omega$ model |
| $\omega$ | Turbulence frequency for the SST $k$-$\omega$ model (1/s) |